

Detection of Boundary Layer Separation and Implementation of
Autonomous Vortex Generators

By

SAMUEL DAVID MORICE

THESIS

Submitted in partial satisfaction of the requirements for the degree of

MASTER OF SCIENCE

in

Mechanical and Aerospace Engineering

in the

OFFICE OF GRADUATE STUDIES

of the

UNIVERSITY OF CALIFORNIA

DAVIS

Approved:

Dr. Stephen K. Robinson, Chair

Dr. C.P. van Dam

Dr. James Baughn

Committee in Charge

2019

CONTENTS

List of Figures	iv
List of Tables	vi
Abstract	vii
Acknowledgments	viii
1 Literature Review	1
1.1 Turbulent Boundary Layer Physics	1
1.2 Computational Methods	6
1.3 Experimental Instrumentation and Flow Visualization	8
1.4 Boundary Layer Control	10
1.5 Stall and Airplane Safety	12
1.6 Summary	13
2 Experiment Introduction	15
2.1 Motivation	15
2.1.1 Aircraft Safety	16
2.1.2 Reduce Parasitic Drag	17
2.2 Objectives	17
2.3 Hypothesis	18
3 Experimental Setup & Methods	19
3.1 Facilities: UC Davis Aeronautical Wind Tunnel	19
3.2 Model: Vertical Span 18" Chord NACA 0012	20
3.2.1 Design	20
3.2.2 Manufacturing	22
3.3 Instrumentation	27
3.3.1 Microphones	28
3.3.2 Data Collection System	29
3.3.3 Tufts	30

3.4	Vortex Generator Activation System	31
3.5	Experiment Design	33
4	Results and Discussion	36
4.1	Fluctuating Pressure Data	36
4.2	Separation Location Using Flow Visualization	39
4.3	Power Spectrum Analysis	40
4.4	Determine Activation Criterion	43
4.5	Real-Time VG Activation	44
5	Conclusions and Future Study	49
5.1	Hypothesis Closure	49
5.2	Future Study	50
List of Symbols		55
Appendices		56
A	Experiment Plan	57

LIST OF FIGURES

1.1	Illustration showing the difference between a laminar velocity profile and a turbulent velocity profile.	2
1.2	Illustration showing the stages of detachment [31].	3
1.3	Illustrations of the three common vortex generator pair configurations. .	12
3.1	Layout of the UC Davis Aeronautical Wind Tunnel [13]	19
3.2	Profile drawing of the NACA 0012 airfoil with the cutouts shown.	21
3.3	Full NACA 0012 wing mounted in the Aeronautical Wind Tunnelb. . . .	22
3.4	The aluminum block with the bandsaw cuts made.	23
3.5	The first side of the airfoil shape milled.	23
3.6	The fixture mounted to the first side of the machined section.	24
3.7	The section fully milled after the finish pass.	24
3.8	Waterjet cutting out the hollow sections.	25
3.9	The setup for drilling the vortex generator mounting holes using a digital level.	26
3.10	The setup for drilling the five microphone mounting holes.	26
3.11	Comparison of the manufactured NACA 0012 airfoil to the classical NACA 0012 airfoil geometry.	27
3.12	Lift performance of the manufactured NACA 0012 test model.	27
3.13	Isometric view of electret condenser microphone used. All dimensions are in millimeters [7].	28
3.14	Middle wing section with microphones installed and labeled.	29
3.15	Teensy 3.5 microcontroller used to collect microphone data.	30
3.16	GUI created to view and record angle of attack.	31
3.17	Tufts mounted near the wing's trailing edge.	32
3.18	A vortex generator with major dimensions.	32
3.19	The vortex generators in their two different states.	33
3.20	Early prototype of the servo motor tray and activation system.	34

4.1	Comparison of the PSDs from MIC 4 at 0° angle of attack and 15° angle of attack obtained during the initial tests done at a Reynolds number of 400,000.	37
4.2	Comparison of the averaged PSDs from MIC 1 at 13° angle of attack and 14° angle of attack at a Reynolds number of 1,000,000.	38
4.3	Comparison of the averaged PSDs from MIC 1 at 15° angle of attack with and without aluminum tape over the microphone at a Reynolds number of 1,000,000.	39
4.4	Results from the computer vision analysis of the tufts.	40
4.5	Peak frequency, PSD peak magnitude and PSD power plotted against the angle of attack for a Reynolds number of 1,000,000.	41
4.6	FFT of the MIC 1 signal at a Reynolds number of 1,000,000 and angle of attack of 0°.	42
4.7	Tufts without the vortex generators turned to their active position. . . .	45
4.8	Tufts with the vortex generators turned to their active position. . . .	46
4.9	Comparison of the PSD power levels at a Reynolds number of 500,000 with and without active vortex generators (VGs).	47
4.10	Comparison of the PSD power levels at a Reynolds number of 1,000,000 with and without active vortex generators (VGs).	47
4.11	Comparison of the lift coefficient curves at a Reynolds number of 500,000 with and without active vortex generators (VGs).	48
4.12	Comparison of the lift coefficient curves at a Reynolds number of 1,000,000 with and without active vortex generators (VGs).	48

LIST OF TABLES

- 3.1 Outline of the wind tunnel tests performed and the purpose of each test. 35

ABSTRACT

Detection of Boundary Layer Separation and Implementation of Autonomous Vortex Generators

Boundary layer separation is a physical phenomenon that can result in aircraft stall, which is responsible for many fatal airplane accidents. This research aims at designing a boundary layer separation detection system that could be added on new aircraft or retrofitted on existing aircraft. This detection system was designed, fabricated, and used to demonstrate an autonomous vortex generator system that detects boundary layer separation in real-time and activates vortex generators to delay the boundary layer separation. The system uses flush-mounted microphones to detect an increase of acoustic power in the low-frequency range of pressure fluctuations indicating incipient separation. Vane-type vortex generators are aligned with the flow until the microphones detect separation. The vortex generators are then rotated to an angle of attack at which they produce vortices that delay boundary layer separation.

Wind tunnel tests are performed with a 2D wing with a NACA 0012 airfoil at chord Reynolds numbers of 500,000 and 1,000,000 in order to characterize the boundary layers frequency domain over a range of angle of attack that includes stall. Results show that the microphones are effective at detecting boundary layer separation and can be used to activate vortex generators. The active vortex generators are shown to increase maximum C_L 13.8% and 6.9% for Reynolds numbers of 500,000 and 1,000,000 respectively when compared to maximum C_L of the clean wing.

ACKNOWLEDGMENTS

I would like to thank Dr. Stephen Robinson for his guidance through this research. Your knowledge and experience has been vital to my success. Thank you to Dr. James Baughn. I appreciate you taking the time to advise me and teach me about aircraft safety and pilot training. I always enjoy hearing about all your flying adventures. Thank you to Dr. C. P. van Dam for your guidance and support with the wind tunnel testing.

To my fellow members of the HRVIP lab, thank you for constantly supporting me and making my time in the lab more enjoyable than I could have imagined. Special thanks go to John Karasinski for all of his advice and guidance. Thank you to Shawn Malone for your valuable assistance with the design and manufacturing of the wing test model. Thank you to Maureen Murphy, Lauren Campbell, Nathan Davis, Kilian Ginnell, and Shannon Geary for all of you help throughout this research.

Last but not least, thank you to my friends and family for always supporting me.

Chapter 1

Literature Review

1.1 Turbulent Boundary Layer Physics

Ludwig Prandtl's paper titled 'On the motion of a fluid with very small viscosity' published in 1904 introduced the concept of the boundary layer [27]. While the concept of the no-slip condition near the wall had been widely accepted by the end of the 19th century, fluid dynamicists and mathematicians still had difficulty accounting for viscosity in the fluid [33]. The introduction of boundary layer theory helped with this problem in fluids with small viscosity. Prandtl discovered that viscosity was not an important factor in the flow except for in a thin layer near the wall. This layer was referred to as the transition layer in Prandtl's paper and later as the boundary layer. In this thin layer, there is a dramatic velocity gradient from the zero velocity at the wall due to the no-slip condition to the freestream velocity. This gradient leads to rotational flow and a region where viscosity cannot be ignored. The flow outside this layer can be approximated as inviscid and irrotational. As a result, inviscid equations could be used outside this thin layer, and viscosity only needed to be accounted for within the boundary layer. Although Prandtl is thought of as the father of boundary layer theory, some scientists had previously introduced concepts that showed the idea of a boundary layer [33]. Notably, William Froude performed experiments on the frictional resistance of water over flat plates in the 1870s [10]. As a result of these experiments, Froude had some idea that there was a layer of intense shear near the wall that grew along the length of the plate.

Boundary layer theory can be divided into two main subsections: laminar and turbulent. While this review mainly focuses on turbulent boundary layers, laminar boundary layers are important to discuss. The fundamental difference between laminar and turbulent boundary layers is the presence of mixing. The mixing in a turbulent boundary layer makes the velocity profile more filled out near the wall as shown in Fig. 1.2. This

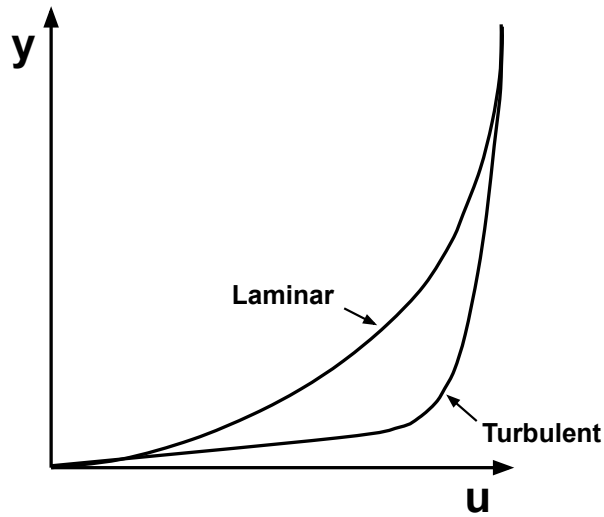


Figure 1.1: Illustration showing the difference between a laminar velocity profile and a turbulent velocity profile.

means that the turbulent boundary layer has more momentum than a laminar boundary layer in that region near the wall. Prandtl performed experiments with spheres that showed that a laminar boundary layer separates earlier than a turbulent boundary layer and subsequently produces more drag [26]. The mixing in a turbulent boundary layer is a result of the complicated structures within a turbulent boundary layer. The presence of these structures in the boundary layer creates complications for computational solutions in the boundary layer. In attached turbulent boundary layers, the coherent structures present are small and low intensity [29]. Turbulent structures are complex and generally unpredictable, so empirical data are crucial for computational solutions.

Prandtl also introduced an explanation of boundary layer separation in his paper. He postulated that this flow separation is likely due to an increase of pressure in the

streamwise direction, referred to as an adverse pressure gradient (APG) [27]. An APG will cause the viscous layer to thicken as momentum is lost to wall shear and the pressure gradient [34]. Eventually the viscous layer will not have enough momentum to resist the pressure gradient, and the flow near the surface will begin to reverse in direction causing the viscous layer to detach from the surface. This results in a region of recirculating flow. Boundary layer separation is defined as the breakaway of the boundary layer which results in a sudden thickening of this viscous region near the wall [31]. This thick region near the wall consists of large eddy structures (large compared to the attached turbulent boundary layer). The point of separation is not easily defined. There are four stages in the boundary layer detachment: incipient detachment, intermittent transitory detachment, transitory detachment, and detachment [31]. The definitions of these stages of detachment are based on the density of instantaneous backflow with respect to time. Incipient detachment is defined as having instantaneous backflow 1% of the time. Intermittent transitory detachment is defined as having instantaneous backflow 20% of the time. Transitory detachment is defined as having instantaneous backflow 50% of the time. Detachment is defined as the point where the time-averaged wall shear stress is zero. Transitory detachment and detachment occur at the same point, and this point is often referred to as the “steady” separation point. This is illustrated in Fig. 1.2.

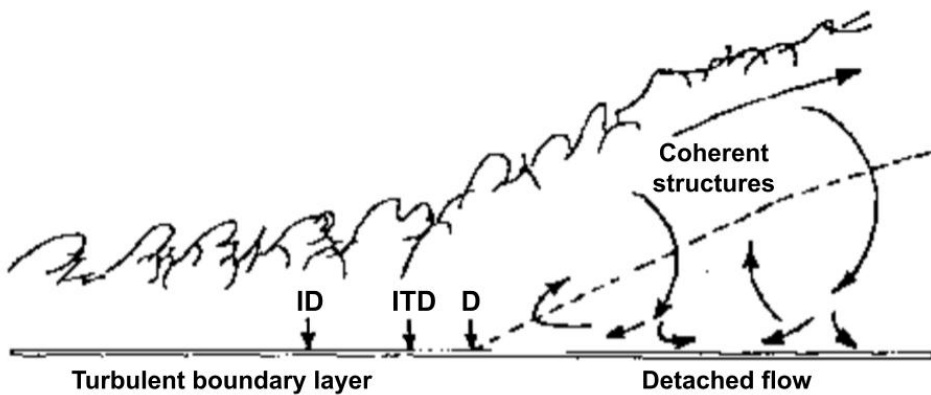


Figure 1.2: Illustration showing the stages of detachment [31].

There are two main types of separation: bubbles and wake-type. Separation bubbles are important to talk about, although this thesis is mainly concerned with wake-type

separation. A separation bubble occurs when the boundary layer separates, forms a region of recirculating flow, then reattaches downstream. This can occur when the boundary layer upstream of the separation point is laminar. When the boundary layer separates, the recirculating flow causes the boundary layer to trip to turbulent. The boundary layer then has enough momentum to resist the APG and reattaches. This is referred to as a laminar separation bubble. Since laminar separation bubbles require a laminar boundary layer, the best way to prevent them is to trip the boundary layer to turbulent. Separation bubbles can also occur in a turbulent boundary layer when the geometry of the surface causes a strong APG Wake-type separation is when the boundary layer never reattaches, and the recirculating region forms a large wake. The characteristic dimension of the region of recirculation tends to be on the same scale as the characteristic dimension of the wing [34]. In the case of an airfoil, that dimension would be the maximum thickness of the airfoil. Wake-type separation contributes a large amount to the drag of a body, causes an airfoil to start losing the ability to produce lift and limits the maximum lift coefficient, $C_{L_{max}}$. Boundary layer separation is a problem in the aviation industry causing aircraft stall which can result in serious accidents [15]. Due to the complexity of boundary layer separation, it is a very difficult topic to study. As such, scientists have been studying the structures in attached and separated boundary layers since their introduction to the scientific community over a hundred years ago.

In ‘The structure of turbulent boundary layers,’ Kline et. al. aimed to investigate the structures in the ‘laminar sublayer’ and the ‘buffer layer’ because these regions account for nearly half of the turbulence production power within the boundary layer [16]. Increasing the understanding of these layers and the physics of the turbulence production in these layers is useful for improving turbulence modeling. The experiments were performed in water channels with a hot-wire anemometer to measure the mean velocity and tiny hydrogen bubbles to visualize the flow and to provide quantitative results. Using these hydrogen bubbles, Kline is able to obtain instantaneous u (streamwise) and w (spanwise) velocity components. With these velocity components, he then finds the instantaneous and average spanwise spectra. These spectra showed that there are fluctuations in the

velocity of a turbulent boundary layer, which cause fluctuations in local pressure. The fluctuation results are obtained very close to the wall. In an attached turbulent boundary layer, these velocity fluctuations and their corresponding pressure fluctuations are small.

Simpson, Ghodbane & McGrath reported on the measurements of surface pressure fluctuation spectra in a separating turbulent boundary layer and link the spectra to the flow field structure in order to learn more for noise prediction techniques [32]. To measure local static pressure fluctuations in the turbulent boundary layer, non-intrusive techniques must be used at the wall. In their experiments, they used sensitive instrumentation microphones that measured the surface pressure fluctuations through pinholes in the test surface. This measurement technique was introduced in this paper. One interesting fact stated in their paper is that the Poisson equation can be used to relate the velocity (u) fluctuations to the pressure (p) fluctuations in an incompressible turbulent flow.

$$\nabla^2 p = -\rho\sigma \quad (1.1)$$

The value σ is defined in tensor notation in Eq. 1.2. The source term σ includes the turbulence and mean-shear interaction in the first term and the turbulence-turbulence interaction in the second term.

$$\sigma = 2 \frac{\partial U_i}{\partial x_j} \frac{\partial u_j}{\partial x_i} + \frac{\partial^2}{\partial x_i \partial x_j} (u_i u_j - \bar{u}_i \bar{u}_j) \quad (1.2)$$

This helps provide an explanation for the high intensity pressure fluctuations present in a separated boundary layer. In a detached boundary layer, it is known that there are relatively large velocity fluctuations that would in turn lead to relatively large pressure fluctuations [31]. The velocity fluctuations near the wall are on the same scale as the freestream velocity [32]. Even in the recirculating region, there is always going to be some forward flow some percentage of the time. The large structures present in the recirculating region have a frequency that varies as U_∞/δ where U_∞ is the freestream velocity and δ is the local boundary layer thickness. The dominant frequency present in the detached region should also be about an order of magnitude lower than the dominant frequency present in the attached boundary layer. This knowledge can help predict the separation frequencies to some degree of accuracy without performing experiments. In an adverse

pressure gradient, the low frequencies scale with the maximum shear stress [20], and East & Sawyer, using empirical data, estimated the maximum shear stress with the shape factor H [8].

$$\frac{\tau_M}{\rho U_\infty^2} = \left[\frac{1}{6.55} \left(1 - \frac{1}{H} \right) \right]^2 \quad (1.3)$$

Panton and Linebarger show large contributions in the spectrum at low frequencies that are due to the large turbulent structures present in the outer region [23]. Since these structures are much larger than the attached boundary layer thickness, the frequency of the pressure fluctuations in the separated region will be dramatically lower than the frequency of the pressure fluctuations in the attached region [31]. On top of the frequencies in the two regions being different, the intensity of the pressure fluctuations will be different due to the difference in the velocity fluctuations between the two regions. The pressure fluctuations in the separated region are also higher intensity than the pressure fluctuations in the attached region. The time-averaged intensity of the pressure fluctuations will gradually increase from incipient detachment to full detachment. The large velocity fluctuations that cause the large pressure fluctuations occur a smaller percentage of the time during incipient detachment than during full detachment. When time-averaged, this would be seen as an increase in intensity as the wing approaches full detachment.

The complicated nature of turbulent boundary layers and boundary layer separation makes them especially important to study with all available resources. Computational methods and experimental methods are both vital to increasing our understanding of the physics in the boundary layer. Boundary layer separation and turbulence present difficult problems to computational methods.

1.2 Computational Methods

There are many problems that arise when trying to model the recirculating region using computational methods. The simplest problem to solve is two-dimensional steady separation [34]. Even in this simplest case, there are still problems that stem from the fact that the attached flow region and the separated flow region have different physical behaviors and length scales. These two regions are divided by a singularity at the separation

point, but information must be transferred between the two regions. One way to simplify the problem is to assume that the recirculating region has a similar length scale as the attached region. This means that just the problems of the singularity and the information transfer between the two regions exist. The singularity issue was addressed by Catherall & Mangler [5] when they prescribed a displacement thickness instead of prescribing the pressure-gradient, which had been the standard until this point. This method solved the singularity issue that was present when the pressure gradient is prescribed. The main shortcoming of this solution was that it encountered issues in the recirculating region due to the fact that the same finite-differencing scheme was used in both the attached region and the recirculating region. This meant that the upstream information did not get transferred downstream to the recirculating region. Another method used to account for the singularity at the separation point was to prescribe a distribution of wall shear as investigated by Klineberg & Steger [17]. Carter [4] also published a paper in which he investigated the last two techniques, prescribed displacement thickness and prescribed wall shear, and compared the results to results obtained by Briley [1]. Carter found very good agreement with each method used.

The issue of the information transfer was also addressed by Klineberg & Steger and Carter [34]. They both changed the solving scheme depending on whether they are solving the equations in the attached region or the separated region. This works because the equation being solved is parabolic in the forward-facing flow region, while the equation being solved in the recirculating region (with backflow present) is parabolic of mixed type. A backward-differencing scheme is used in the attached region; but when backflow is present, a forward-differencing scheme must be used to ensure that the information is flowing in the correct direction. These methods are all applicable to laminar separation. Turbulent separation adds the issue of accurately modeling turbulence, a problem that still exists. This is where experimentation becomes especially important. Turbulence models are heavily based on empirical values meaning that a very large body of experimental data for turbulent separation is necessary to produce accurate and reliable turbulence models.

1.3 Experimental Instrumentation and Flow Visualization

When performing experiments concerning boundary layers, it is difficult to measure the flow characteristics very close to the wall. Anemometers are one of the best instruments to use when studying boundary layers. A couple of popular anemometers for wind tunnel testing are hot wire anemometers and laser Doppler anemometers (LDA). These tools are valuable because they can measure velocities very accurately through the entire boundary layer. These anemometers are especially valuable for measuring velocity fluctuations and turbulence levels in fluids due to their extremely high frequency response and sensitivity.

Hot wire anemometers first appeared in the late 1800s, became more sophisticated throughout the 1900s, and are now used for a wide range of applications. For wind tunnel experimentation, they were originally only used for measuring mean velocities, but later they started being used for measuring velocity fluctuations [6]. The typical hot wire is very small, on the scale of 1 mm long and $5\mu\text{m}$ in diameter, making them great for boundary layer measurements as they will not greatly disturb the flow in the boundary layer. These wires tend to be made of tungsten or platinum [19]. Due to the small diameter of these wires, they are extremely fragile. Hot wire anemometers have a very desirable frequency response, up to 400 kHz typically. They offer high sensitivity, high spatial resolution, and an easy-to-read output signal making them an extremely versatile instrument [19]. However, hot wires can be costly, are very delicate, and require a lot of time to prepare and maintain.

Laser Doppler anemometers are nonintrusive, which is especially important when working with boundary layers. They consist of a laser, a beam divider, and a collector. LDA systems have similar characteristics to hot wire anemometers. Since an LDA is an optical system, it does not need to be inserted into the boundary layer unlike the hot wire system. Although LDA systems are valuable, they do have their disadvantages. LDAs are expensive instrument setups. In order to study multiple points in the flow field, the entire LDA setup must be moved, and there must be optical access to the entire flow field being studied [14]. The anemometers used in wind tunnel testing are very useful

when studying the detailed physics and structures of boundary layers but are not feasible for applications involving an aircraft.

Particle image velocimetry (PIV) is a more recent development in velocity measurement systems. PIV is very useful when velocity measurements from the entire flow field is necessary. The PIV technique is also extremely fast, on the scale of seconds. The PIV system consists of a laser and associated optics, imaging optics, and tracer particles seeded into the flow [28]. Like LDA systems, PIV systems are nonintrusive. PIV works by taking many images of the laser-illuminated tracer particles, and using statistical methods to track the particles from one image to the next. Using the known time delay between images and length-scale in the image, a quantitative velocity vector can be determined. PIV can also be used for qualitative flow visualization. PIV does require specialized equipment and full optical access to the flow field making it impractical for some applications. Flow seeding is also challenging. The choice of the seeding material depends on its visibility and toxicity. It is also possible to use LDA and PIV for sound measurements [3].

Pressure systems are also extremely valuable for studying fluid flows. A common pressure measurement tool for determining air velocity is the pitot tube. Pitot tubes use the relation between static pressure and stagnation pressure to determine the airspeed. Pitot tubes are extremely common in wind tunnels as well as on aircraft. Pressure taps are commonly used to measure local static pressure. Arrays of pressure taps around the surface of an airfoil are often used to determine the coefficient of pressure distribution and subsequently the 2D lift of the airfoil. Microphones are valuable when the frequency domain of the pressure data is desired. There are a wide range of microphones available with various accuracies, frequency responses, and sensitivities. Electret microphones can be cheap and small and can be used for pressure fluctuation measurements [30]. An electret microphone is a type of condenser microphone that has a permanently charged thin film that removes the need for external power.

Flow visualization is important for scientists to get a general insight into the physics of a fluid flow. Common flow visualization tools used for aeronautical experiments are smoke lines, oil flows, tufts, and tracer particles [21]. Tracer particles have already been

mentioned for PIV. Smoke lines are useful when studying the streamlines around a rigid body and for the wake behind a rigid body. Careful consideration must be taken to use the proper smoke when using this visualization tool, as it needs to be visible, nontoxic and must be able to resist mixing and diffusion in the flow. Oil flow on the surface is useful for determining the surface shear stress directions on the entire surface of the body being studied. A pigment powder is added to an oil which is then distributed on the surface of the body. When the body is exposed to the flow, the pigment will leave deposits that show the direction of flow. Surface oil flow is particularly useful for showing transition regions and separation points. It has the added benefit that the patterns do not go away after the flow is turned off. One downside of oil flow is that it can be very messy. The oil often will fly downstream of the model and can coat the inside of the wind tunnel. Tufts are one of the simplest flow visualization techniques. Tufting involves placing a grid of strings, or tufts, on the surface of the model. When the flow is turned on, the tufts will indicate the local direction of flow. Tufts are useful for showing flow separation happening in real time. Tufts in a separated region of flow will flip around and violently flutter in the upstream direction.

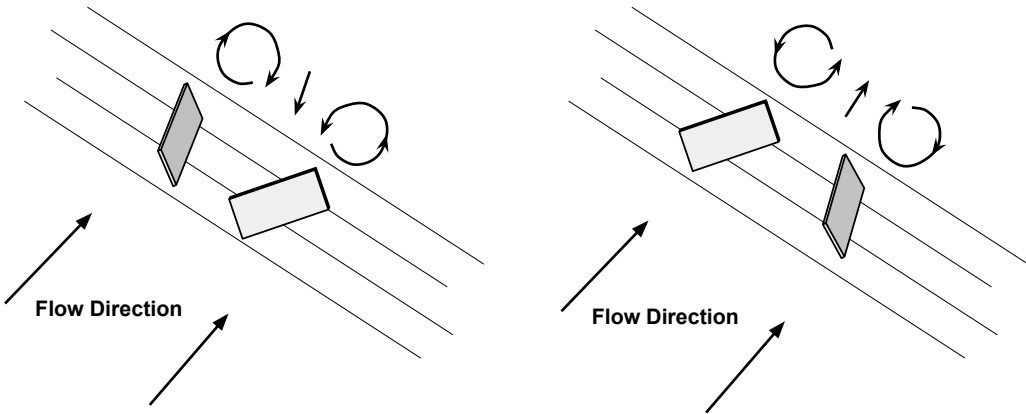
1.4 Boundary Layer Control

There are many forms of flow control, but the main focus in this review will be on flow control with the purpose of delaying boundary layer separation. Flow control methods can be divided into two main types: active and passive [11]. Active flow control methods require some sort of energy input from an outside source while passive methods do not. While active methods are effective, they add a failure point to a critical safety system on aircraft and thus are not often used outside of experiments. Passive methods increase drag in order to increase the energy in the boundary layer. The three most common active methods are suction, wall cooling, and blowing. Suction works best when implemented in the separated region. It works by removing the low momentum flow from the near-wall region of the boundary layer and keeping the boundary layer thin and attached. Suction can also be a passive system, but this is most effective in supersonic flows. Wall cooling

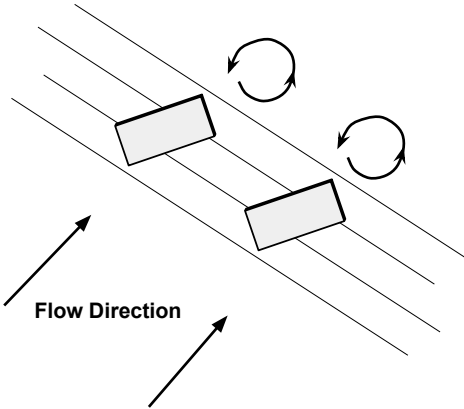
works in gases by increasing density and decreasing viscosity. This is another method of manipulating the velocity profile. Due to the decrease in viscosity, the velocity increases closer to the wall which means that the boundary layer will be able to resist the adverse pressure gradient longer. Blowing is an active method that adds momentum to the near-wall portion of the boundary layer. The increase of momentum in the boundary layer increases its ability to resist the APG. Passive blowing is often used in high lift systems to increase the effectiveness of the system and to prevent separation on the flaps.

One of the simplest passive methods for delaying boundary layer separation is to ensure the boundary layer is tripped to turbulent. Laminar boundary layers are not as good at resisting the adverse pressure gradient as turbulent boundary layers due to the increased momentum near the wall caused by mixing in a turbulent boundary layer. Of course a friction drag penalty is incurred by the turbulent boundary layer. The most common passive method of controlling boundary layer separation on airplanes is vane-type vortex generators. Vane-type vortex generators are small vertical vanes that are mounted at an angle of attack relative to the freestream velocity. At this angle of attack, the vortex generator has low pressure flow on one side and high pressure flow on the other causing the high pressure fluid to curl over the vortex generator to the low pressure side. In the presence of the freestream flow, this results in a vortex downstream of the vortex generator. This vortex entrains fluid from outside the boundary layer and adds momentum to the boundary layer [22]. Vane-type vortex generators can come in several different configurations: counter-rotating common flow down, counter-rotating common flow up, and co-rotating. Figure 1.3 shows these three vortex generator pair configurations. For the purpose of controlling boundary layer separation, a counter-rotating common flow down configuration is accepted as the most effective [25]. This is because the common flow going down forces the most momentum down into the boundary layer. The counter-rotating common flow up configuration is not as effective at delaying separation because the momentum in the flow is not increased near the surface.

While effective at delaying boundary layer separation, vortex generators are always active and incur a drag penalty even when not needed. Research was done on micro-



(a) Counter-rotating common flow down. (b) Counter-rotating common flow up.



(c) Co-rotating.

Figure 1.3: Illustrations of the three common vortex generator pair configurations.

vortex generators that can be mounted on the leading edge of a flap [18]. When the flaps are stowed, the vortex generators are also stowed.

1.5 Stall and Airplane Safety

Although boundary layer separation has been extensively studied, it is still a prevalent issue in the aerospace industry. Stall is a dangerous aspect of airplane flight. Stall accidents account for nearly 25% of fatal airplane accidents and nearly 50% of all stall accidents are fatal [15]. Stall warning systems currently available on airplanes do not actually sense boundary layer separation or anything to do with the physics of stall.

Instead, stall warning systems rely on angle of attack sensors and data on the stall angle of attack. The stall warning systems, such as warning lights and stick shakers, do not do anything to delay the boundary layer separation. They will warn the pilot that the airplane is approaching stall, and in commercial applications they may activate automatic systems to get the airplane out of the stall region. Even with automatic systems, the pilot still needs to react to the situation quickly and correctly to recover from the stall safely. In some stall situations, this can be extremely difficult. One such stall situation is the yawed stall. When the airplane is yawed, one wing will be more swept back than the other causing this wing to stall before the other wing. With only one wing stalled, a large rolling moment is applied to the airplane, and the airplane can put into a spin. More than 66% of stall accidents occur on personal flights indicating a lack of pilot training. Inexperienced pilots can unknowingly get into stall situations without any prior indication of stall [15]. Stall accidents are more common during takeoff and initial climb during personal flights making up 26% of personal flight stall accidents. Takeoff and climb is also the most fatal flight regime for stall accidents with nearly 40% of stall accidents occurring during takeoff and climb resulting in fatalities.

While stall accidents are far more common during personal flights, they do still occur on commercial flights. In October 2018 and March 2019, two Boeing 737 MAX airplanes crashed shortly after takeoff. These crashes were attributed to the erroneous activation of the Maneuvering Characteristics Augmentation System (MCAS). The MCAS function was implemented to prevent imminent stall by pushing the nose down after stall was detected. The MCAS uses a angle of attack vane to indicate stall, but in the cases of the two accidents, the angle of attack sensor reportedly malfunctioned and erroneously activated the MCAS. This demonstrates how important stall detection is, and how it is still an issue in modern airplanes.

1.6 Summary

Although the field of boundary layer theory is over a hundred years old, there is still a lot that is not known or fully understood about boundary layers. This makes it an

important and interesting field to study. Particularly interesting subjects in boundary layer theory are turbulent boundary layer separation and the structures present in a separated boundary layer. Computational fluid dynamics (CFD) has difficulties modeling turbulent boundary layers and boundary layer separation due to the complicated and stochastic nature of the structures present in these flows. This means that experiments are vital to further the understanding of turbulent boundary layer separation. Previous experiments have demonstrated that the large structures in a separated boundary layer cause low frequency surface pressure fluctuations.

Turbulent boundary layer separation is especially important to understand because of the applications to the aircraft industry. Boundary layer separation can cause airplane stall, which results in many fatal accidents. The use of flow control devices to delay boundary layer separation is common on airplanes. The most common flow control device is the vortex generators. Vortex generators work by adding momentum to the boundary layer, making the boundary layer better able to resist separation. However, vortex generators add drag to the aircraft. This provides an incentive to research methods to activate vortex generators only when they are necessary.

Chapter 2

Experiment Introduction

2.1 Motivation

Turbulent boundary layers are complex and difficult to simulate accurately. Experimental studies of boundary layers are valuable to the academic community in fluid dynamics. More experimental knowledge of the physics of turbulent boundary layers and their detachment is always needed to improve current computational models. While there has been a lot of research concerning the pressure fluctuations in a separating boundary layer, much of the research investigating the surface pressure fluctuations have ignored the low frequency region of their signal due to the fact that the wind tunnels they were using have a low-frequency resonance. Previous research has been done by Louis Edelman at the University of California, Davis on the concept of using small electret microphones, similar to the microphones used in cell phones, to detect boundary layer separation [9]. Edelman performed wind tunnel tests with a modified S819 airfoil model which showed that electret microphones can be used to detect a change in the frequency domain as a result of boundary layer separation. Edelman's research was used as a springboard for this thesis as it showed that the low frequency pressure fluctuations due to separation have a much larger power density than the low frequency resonance present in the wind tunnel. There is value to studying these low frequency surface pressure fluctuations as they make up the majority of the sound signal in a separated boundary layer. Besides the scientific value of studying the pressure fluctuations in a separating boundary layer,

there are real-world applications of these findings. These pressure fluctuations are unique to boundary layer separation and could be used to indicate incipient detachment. This thesis focuses on using the low frequency pressure fluctuations to indicate an approaching stall and to implement a reactive flow control system that increases aircraft safety by delaying the boundary layer separation.

2.1.1 Aircraft Safety

Inadvertent stall situations are very risky and cause a significant portion of personal airplane accidents. These accidents are often due to a lack of training and experience among the pilots. Many of the stall situations that are encountered require fast and accurate responses from the pilot in order to recover from the stall. If the pilots are inexperienced, they may not respond appropriately in a timely manner to recover before it is too late. An auxiliary safety system that delays boundary layer separation could buy just enough time for the pilot to react correctly and get out of the stall situation. This thesis investigates a safety system that could do just that. To be most effective, this system would be completely autonomous and would not require any pilot input. Since inadvertent stalls are often due to pilot distractions, adding another distracting task for the pilot to complete would only make the situation worse for the pilot. While the system would not need any input from the pilot to activate, it could also act as an early warning system for the pilot.

A system based on the physics of stall could not only act as a more consistent warning system but also could indicate if stall is occurring only on one wing or on a specific region of the wing. Stall occurring on one wing is especially dangerous because it can lead to a sudden rolling moment that can be difficult to recover. Another dangerous stall situation that can occur is when the tip of the wing stalls causing the ailerons to lose effectiveness. This can lead to loss of control of the aircraft. Both of these localized stalls are not necessarily detected by angle of attack sensors and can occur unexpectedly if the pilot is inexperienced or distracted.

On top of being an early warning system for the pilot, the system can activate flow control devices to delay boundary layer separation where it is happening. The flow control

devices most common on airplanes are vane-type vortex generators (VG), and vortex generators affect a very specific region of flow downstream of the VGs. This can make the flow control very customizable with only the separating regions being affected.

2.1.2 Reduce Parasitic Drag

As mentioned previously, passive flow control systems are effective at delaying boundary layer separation, but they do come with a parasitic drag increase. The vortex generators currently used on airplanes are always producing vortices and are thus increasing the overall parasitic drag of the aircraft. While this increase in drag is small, airplane manufacturers are always looking for ways to decrease drag. A reduction in drag leads to better fuel efficiency and more passenger capacity. It has been suggested that reducing the drag of a large commercial aircraft such as the Boeing 747 by one drag count can allow the aircraft to carry one more passenger. Airframe manufacturers and airlines benefit from any drag reduction that they can get. Having a system that only activates the vortex generators when and where they are needed can help decrease drag.

2.2 Objectives

To be feasible for use on an airplane, the separation control system proposed in this thesis would need to be lightweight, reliable, and low-cost. With those limitations in mind, a reactive flow control system has been designed and tested in a wind tunnel. The objective of this thesis is to design and implement an autonomous vortex generator system that activates when trailing edge boundary layer separation is detected. This system must be modular and adaptive so that it can be easily implemented into modern aircraft without complex physical models or redesign of the aircraft. Also, the system will not require any intervention from the pilot to activate which will provide the pilot more time to react to the stall situation correctly. This objective can be broken down into two main parts: detection of the boundary layer separation and activation of the vortex generators. A detection criterion must be determined before it is possible to activate the vortex generators at an appropriate time. Once the detection criterion is determined, it must be demonstrated to work in a real-time experiment.

2.3 Hypothesis

This thesis aims to test and demonstrate the following hypothesis: boundary layer separation can be detected in real time by analyzing the frequency spectra of surface pressure fluctuations for an increase of the power density in the low frequencies. This hypothesis will be tested with wind tunnel tests run at chord Reynolds numbers of 500,000 and 1,000,000. The frequency spectra will be obtained using inexpensive microphones to record the surface pressure fluctuations present near the trailing edge of the wing.

Chapter 3

Experimental Setup & Methods

3.1 Facilities: UC Davis Aeronautical Wind Tunnel

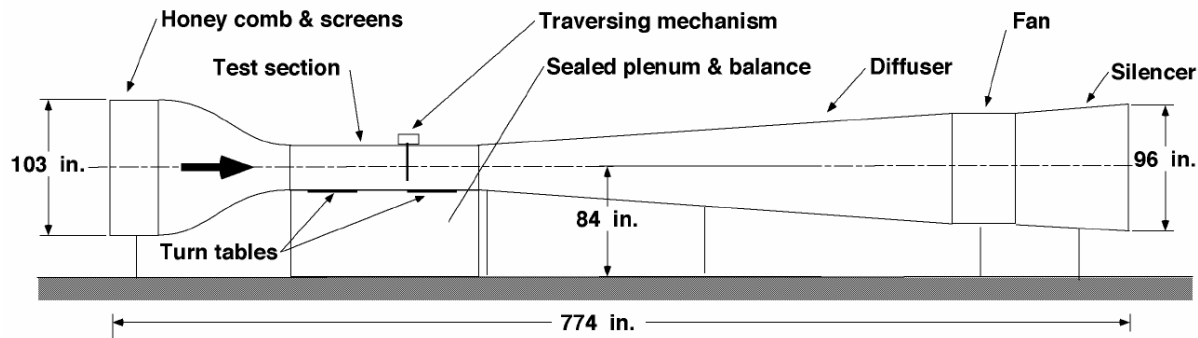


Figure 3.1: Layout of the UC Davis Aeronautical Wind Tunnel [13]

All experiments for this thesis were done in the UC Davis Aeronautic Wind Tunnel (AWT). The UC Davis Aeronautic Wind Tunnel is a low turbulence, open-circuit wind tunnel made by Aerolab. The test section measures 33.6" x 48" x 12'. The contraction section has a contraction ratio of 7.5:1 with an inlet that measures 103" x 103". The inlet has a course debris screen, a 6" honeycomb layer, and four fine anti-turbulence meshes. A 125 hp fan pulls the air through the test section with a max velocity of 165 mph. The wind tunnel has a pyramidal balance that measures the three forces and three moment components that the model experiences. The side force, lift for vertically mounted models, can be measured up to 150 lb.

Before testing began, microphone measurements were taken with the wind tunnel off to

see if there was any significant acoustic or electrical noise present. Electrical noise spikes were observed at 60 Hz and 120 Hz, and we therefore installed shielding on the lengths of the wires in order to reduce this electrical noise. After the shielding was installed, microphone measurements showed that some of the noise was removed. Measurements were then taken with the wind tunnel on and the wing model at 0° angle of attack. A Fast Fourier Transform (FFT) was performed on the microphone data to transform the data into the frequency domain. The results revealed that there were not any dominate frequencies present, and the FFT looked like that of white noise. This showed us that the wind tunnel would work for our purposes, despite not being a “low-noise” wind tunnel.

3.2 Model: Vertical Span 18” Chord NACA 0012

Prior to beginning wind tunnel testing, a new wing needed to be made. The only other model with the room for the instrumentation required for these experiments was the modified S819 airfoil used for Edelman’s previous research [9]. While this wing was fine for the initial experiments, it had some characteristics that were undesirable for further testing. First, the S819 is a stall-regulated airfoil so the stall characteristics are very mild. We wanted a wing that had more dramatic stall characteristics as we were aiming to study the stall region. Second, the only way to mount the microphones was through the pinhole pressure taps which required tubing to step down from the microphone size to the pressure tap size. While Edelman did account for the transfer function and frequency response of this step-down tubing, we wanted to install flush mounted microphones to ensure that we are measuring only the pressure fluctuations in the separated boundary layer instead of some resonant frequencies of the tubing. Based off these concerns, we decided to manufacture a new 18” chord wing for these tests. We chose a NACA 0012 airfoil for its test heritage and its dramatic stall characteristics.

3.2.1 Design

The model is mounted vertically in the AWT and has a span of 33.125” and a chord of 18”. The model consists of seven 4.625” tall sections, a 0.25” top cap, and a 0.5” mounting plate. The model is constructed of 6061-T6 aluminum, and each section is machined from

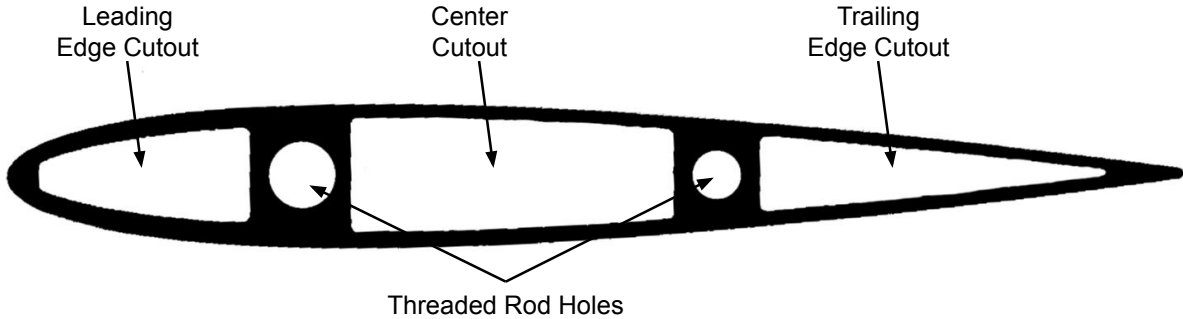


Figure 3.2: Profile drawing of the NACA 0012 airfoil with the cutouts shown.

a single block of aluminum. In order to lighten the model and provide room for the instrumentation, the top six sections have three cutouts as shown in Fig. 3.2. To reduce the tool chatter during manufacturing, the trailing edge has a $1/16''$ radius. While this rounded trailing edge does have an effect on the aerodynamics of the wing and the trailing edge noise [2], it was decided that the reduced tool chatter and thus improved surface quality outweighed the aerodynamic effects of the rounded trailing edge. The leading edge cutout does not house any instrumentation for this experiment, but it was added to lighten the model and to allow for instrumentation in future experiments. The center cutout houses the vortex generator activation system, and the trailing edge cutout houses the flush mounted microphones. For this experiment, only the middle of the seven wing sections is instrumented with five flush-mounted microphones, and two rotating vane-type vortex generators.

The bottom section is left solid for mounting purposes. The seven sections are stacked together using three dowel pins in between each section to ensure that all sections are aligned with each other. Two $33''$ threaded rods are then used to squeeze all the sections together. These threaded rods also act as the main structure components of the model. They are made of steel and can withstand the maximum forces that the model would ever see. The fact that all the sections of the model are compressed together also adds significant rigidity to the model. The top cap and bottom mounting plate are then bolted to the ends of the model. The full model is then mounted to the force balance in the AWT as shown in Fig. 3.3.

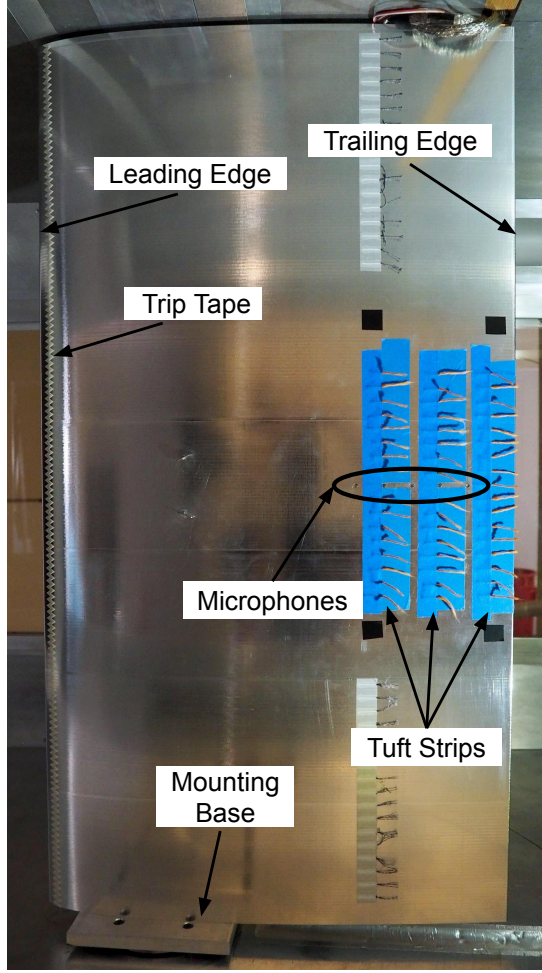


Figure 3.3: Full NACA 0012 wing mounted in the Aeronautical Wind Tunnel.

3.2.2 Manufacturing

The wing model was completely manufactured at the UC Davis Engineering Student Design Center (ESDC) under the guidance of Assistant Development Engineer Shawn Malone. Each section was machined on a Mori Seiki DMC 1035v 3-axis mill, and then an OMAX 55100 waterjet was used to cut out the hollow sections. The manufacturing process was designed by UC Davis MAE undergraduate students, Maureen Murphy and Lauren Campbell, under the guidance of Shawn Malone. All the fixtures (milling fixtures and waterjet fixture) were designed and manufactured by Lauren Campbell using a Mori Seiki 3-axis mill and a Mori Seiki 5-axis mill. These fixtures were important for ensuring that each section would line up with each other when stacked together.

We started with a solid block of aluminum. Cuts were made on a bandsaw to remove



Figure 3.4: The aluminum block with the bandsaw cuts made.



Figure 3.5: The first side of the airfoil shape milled.

as much material from the solid block as possible before milling as shown in Fig 3.4. This was done to reduce the milling time. Once the bandsaw cuts were made, the block was secured in the mill using two vises. The airfoil shape was then roughly cut into the top half of the block, and mounting holes and dowel pin holes were drilled in the top surface as shown in Fig. 3.5. The dowel pin holes were used to align the block onto the next fixture, and the mounting holes were used to secure the block to the fixture as shown in Fig 3.6. The fixture and the block were mounted back into the machine, and the airfoil shape was cut into the other half of the block. Once the entire section had the airfoil shape roughly cut, a finish pass was done to cut the exact profile of the NACA 0012 on the entire section.

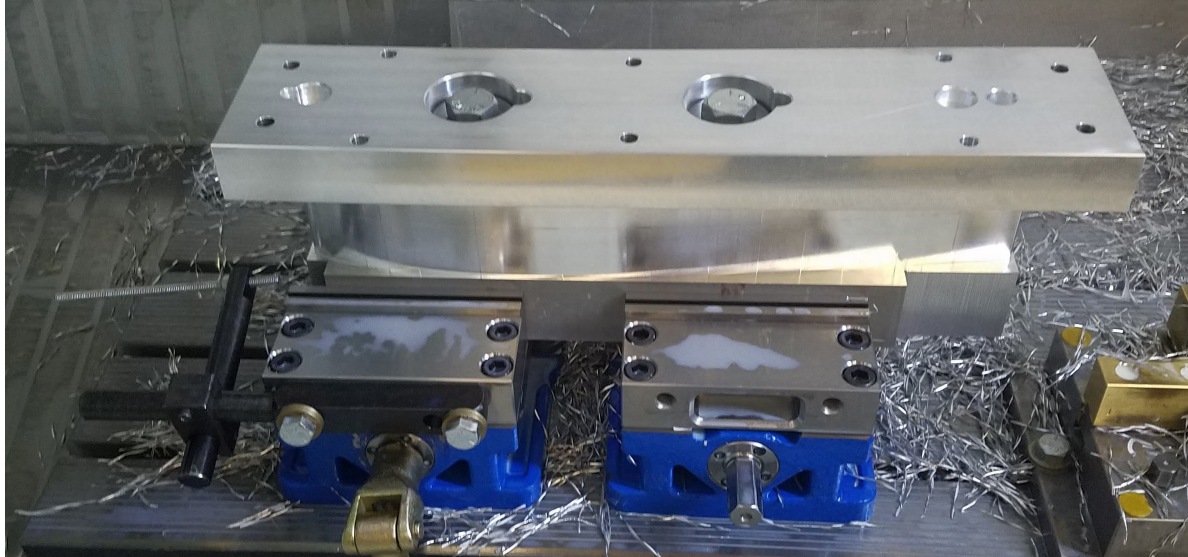


Figure 3.6: The fixture mounted to the first side of the machined section.

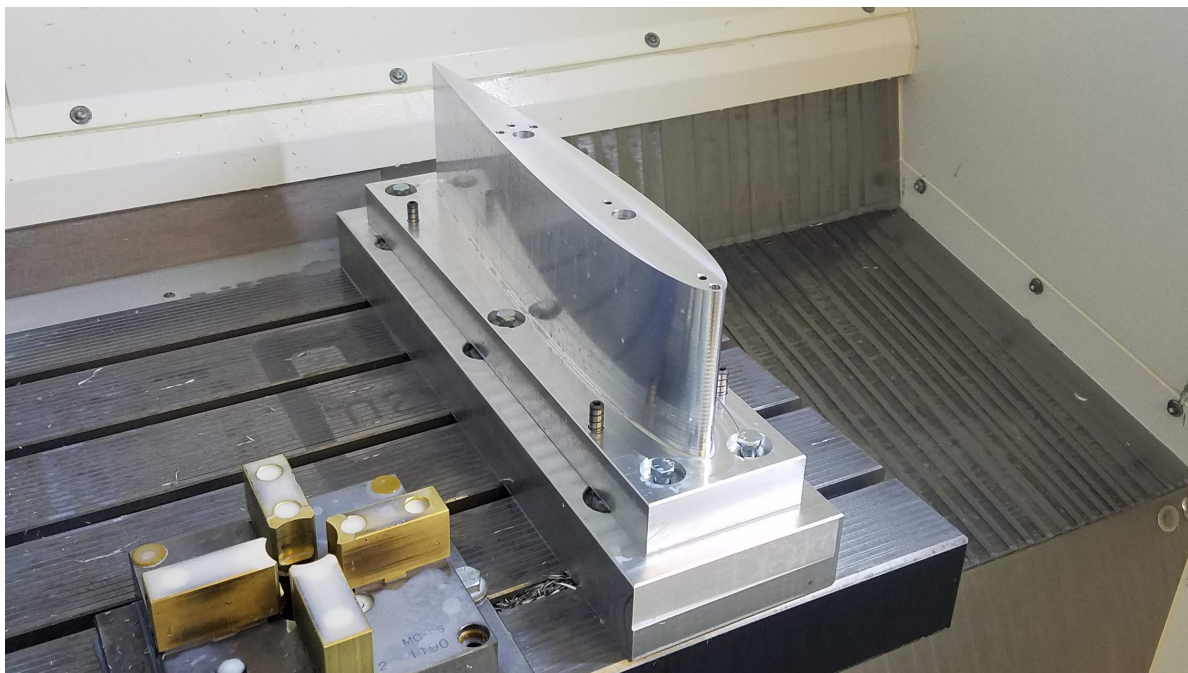


Figure 3.7: The section fully milled after the finish pass.

The finish pass also ensured that the model has a smooth surface finish as the smaller cut reduces tool chatter as the cut was made. The fully milled section is shown mounted in the mill in Fig 3.7. Once the section was fully milled, the hollow cutouts needed to be made on the waterjet. The model was mounted to a fixture made for the waterjet cuts and secured on the waterjet table as shown in Fig 3.8.



Figure 3.8: Waterjet cutting out the hollow sections.

For the middle section, it was important to drill the vortex generator mounting holes and the microphone mounting holes perpendicular to the surface. The holes for the microphones had a diameter slightly larger than the diameter of the microphones to allow for the microphones to be inserted without large gaps around them. A digital level was used to set up the model so that the surface was perpendicular to the drill at the point where the hole was being drilled. This setup can be seen in Fig. 3.9 and Fig. 3.10

Once the wing was manufactured, the profile shape needed to be verified as a NACA 0012 airfoil. The first manufactured section was verified to be a NACA 0012 by measuring the outer profile with the MicroVu Excel 502HC measurement machine. The measured profile was then digitally compared to the classical NACA 0012 equation as shown in Fig. 3.11. After the first manufactured section was confirmed to match the NACA 0012 airfoil, the rest of the sections were machined.

Once the full model was completed and mounted in the wind tunnel, the force balance was used to measure the lift of the wing and a C_L vs. α curve was plotted. Figure 3.12 shows the plot produced. The angle of attack was corrected so that zero lift corresponds to zero angle of attack. (A slight discrepancy was caused by the fact that the model could not be mounted exactly at an angle of attack of zero degrees.) The lift curves show substantial 3D effects on the wing. While the gap between the top of the wing and the



Figure 3.9: The setup for drilling the vortex generator mounting holes using a digital level.

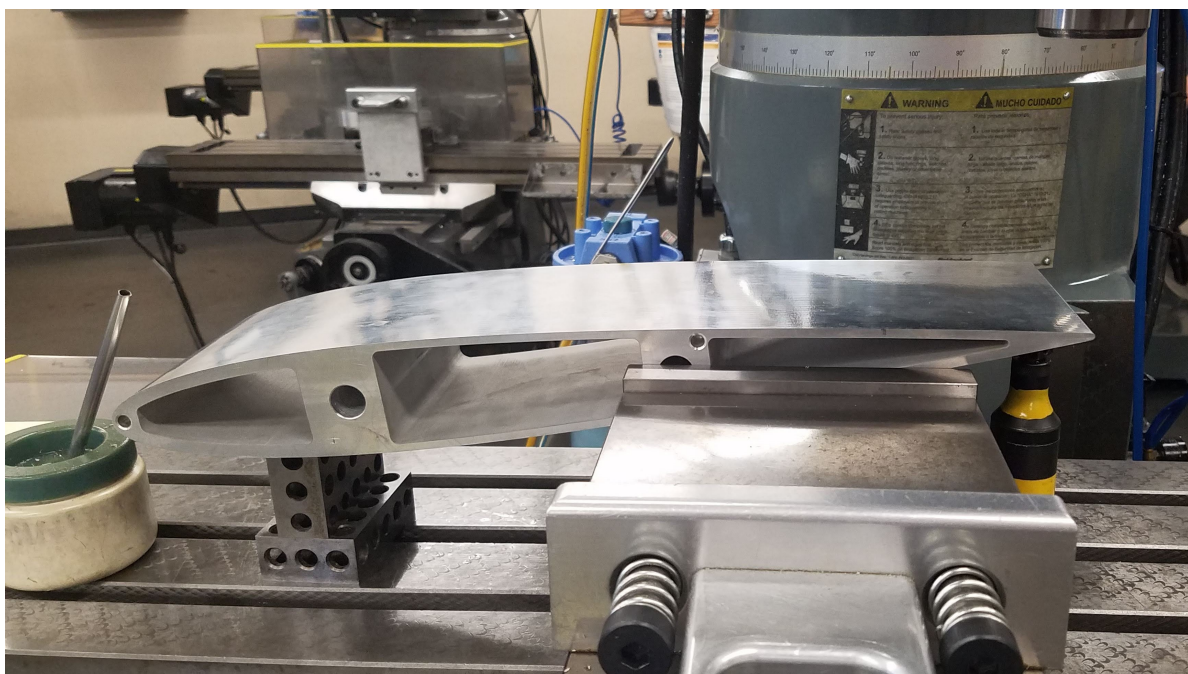


Figure 3.10: The setup for drilling the five microphone mounting holes.

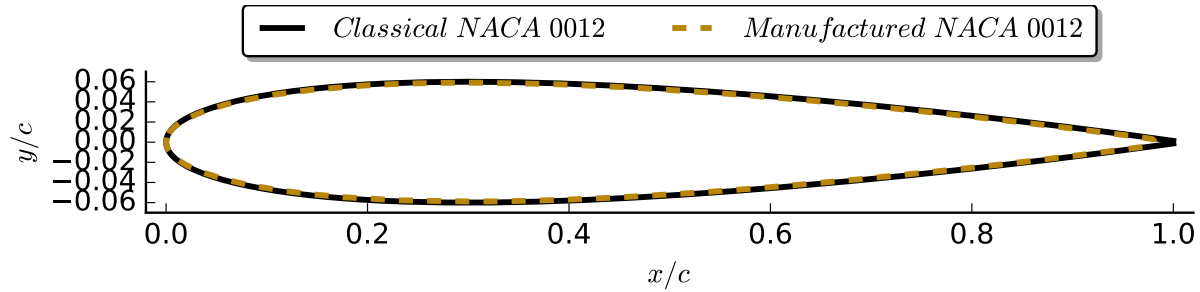


Figure 3.11: Comparison of the manufactured NACA 0012 airfoil to the classical NACA 0012 airfoil geometry.

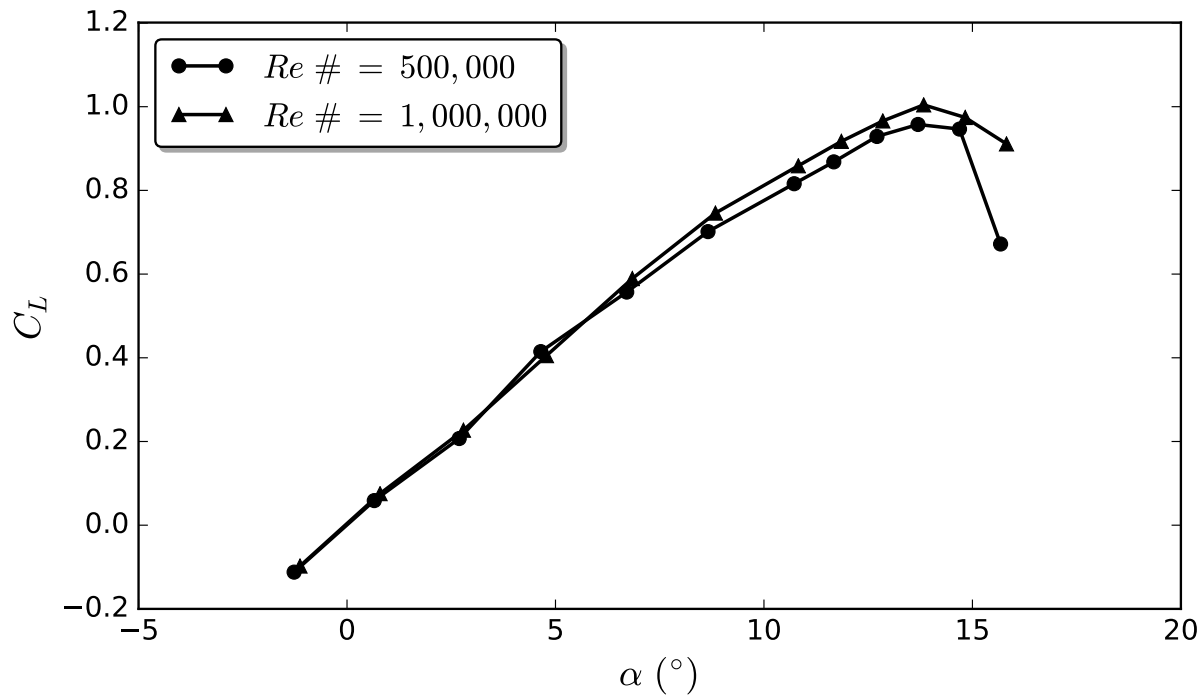


Figure 3.12: Lift performance of the manufactured NACA 0012 test model.

wind tunnel wall is small, the gap at the bottom of the wing is large enough to allow some transverse flow to occur on the wing. Tufts mounted near the bottom of the wing showed this transverse flow. They also showed that the transverse flow does not affect the middle of the wing where the microphones are mounted.

3.3 Instrumentation

When choosing the instrumentation for these experiments, we first needed to decide what to prioritize. We needed flush-mounted microphones, a way to record the data from the microphones, flow visualization, and the vortex generator activation system. One

of our priorities was to keep the separation detection and VG activation systems light weight, compact, and low cost in order to demonstrate that this type of system could be easily adapted to a real-world application. Another priority was to measure the pressure fluctuations in a chordwise region near the trailing edge and to visualize the flow in that same region.

3.3.1 Microphones

The microphones needed to be small, lightweight and inexpensive. We decided to use electret microphones similar to those used in cell phones because of their low cost and relatively good sound quality. The particular microphones chosen are the MO044402-6 electret condenser microphones by DB Unlimited. An isometric view of this microphone is shown in Fig. 3.13. These microphones have a flat frequency response from 40Hz to 20kHz.

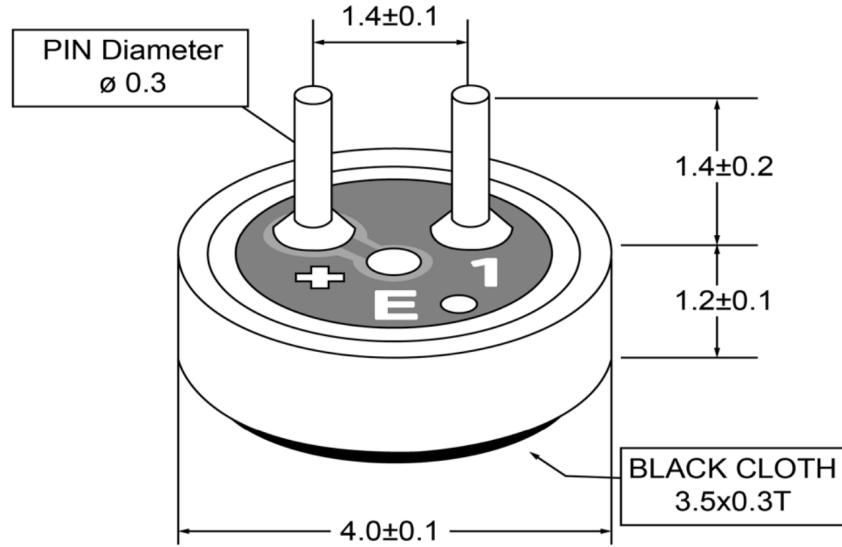


Figure 3.13: Isometric view of electret condenser microphone used. All dimensions are in millimeters [7].

Frequencies below 40 Hz will be attenuated due to the microphone's small diaphragm.

The microphones are soldered to lead wires that are connected to signal amplifiers. The amplifiers used are the Maxim MAX9813 electret microphone amplifiers with automatic gain control with a maximum gain set to 40dB. The amplifiers are necessary because the electret microphones do not produce a voltage difference large enough to measure alone. The microphone is then flush mounted into the middle section of the wing and secured in

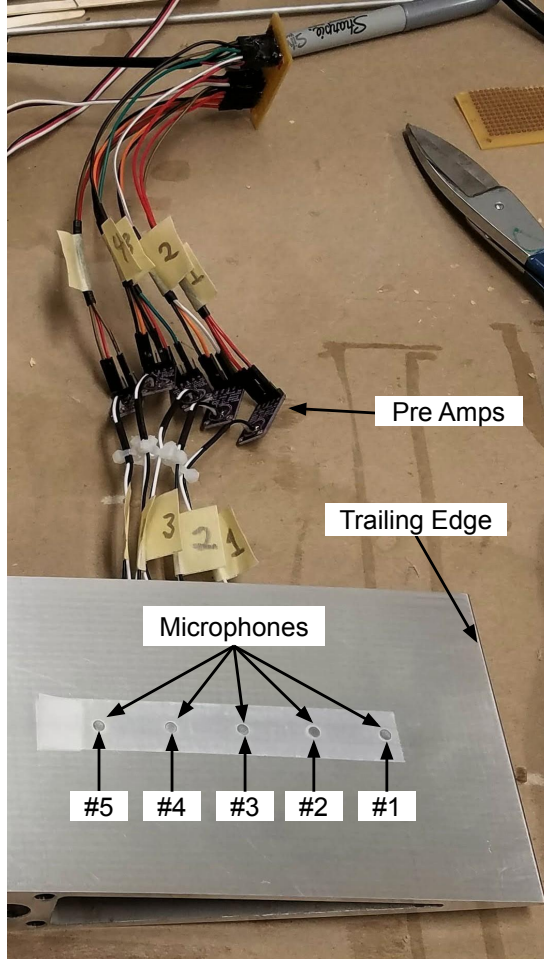


Figure 3.14: Middle wing section with microphones installed and labeled.

the model using silicone adhesive as shown in Fig. 3.14. As labeled, MIC 1 is 1.75" from the trailing edge and the microphones are 1" apart. The microphones were mounted flush with the surface so that they would not disturb the flow in any way. If a microphone were mounted below the surface, a cavity flow would develop that would have its own frequency characteristics separate from the rest of the flow.

3.3.2 Data Collection System

The main data collection system consists of five electret microphones, in-line amplifiers for each microphone, and a Teensy 3.5 microcontroller. The Teensy 3.5 was chosen because of its high processing speed and its capability to store data directly to a MicroSD card. This system recorded a “snapshot” of 5000 samples from each microphone at a rate of

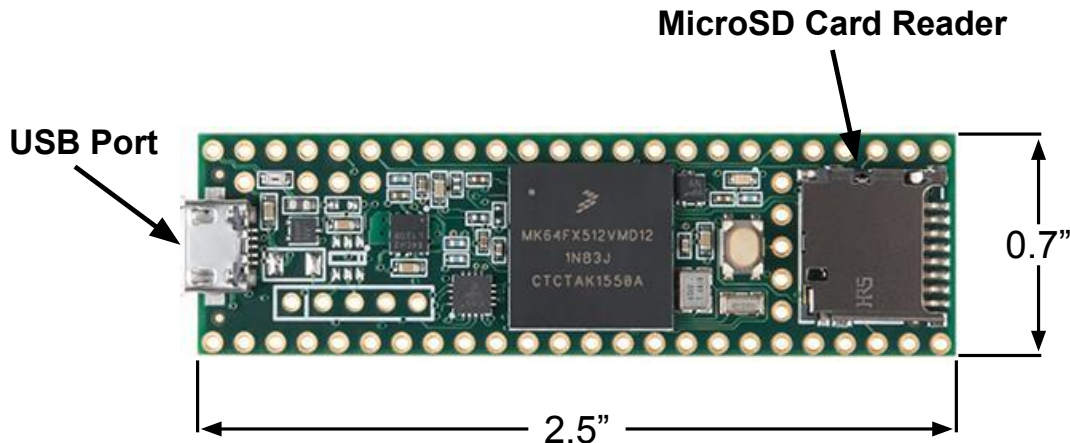


Figure 3.15: Teensy 3.5 microcontroller used to collect microphone data.

7500Hz per microphone, dumped those samples to a data file on the MicroSD card, and then repeated this until 15 “snapshots” were recorded. The Teensy 3.5 also handles the analysis and determination of separation in the second part of the experiment.

We used a separate Teensy LC microcontroller to read the angle of attack data from the wind tunnel turntable potentiometer. The voltage from the potentiometer was fed into the microcontroller and converted to angle of attack after a calibration was performed. A Graphical User Interface (GUI) was designed with a real-time scrolling plot and readout of the angle of attack so that the angle of attack can be accurately set during the experiments. The GUI also handles calibration and data recording. Figure 3.16 shows the GUI.

The force balance and airspeed data are recorded with LabVIEW. These data are taken at 3000 Hz with every 1000 samples averaged. After averaging, 100 data points are recorded.

3.3.3 Tufts

Tufts were used to visualize the flow and to provide a confirmation of separated flow. Several methods of flow visualization were considered, but tufts were chosen because of their simplicity and acceptance in the testing community. The tufts are 1” long and spaced 0.5” apart in the spanwise direction. Since the tufts are surrounding the microphones, there was some concern about the fluttering tufts causing some additional noise. Tests were done with and without the tufts to confirm that the tufts do not have any effect on

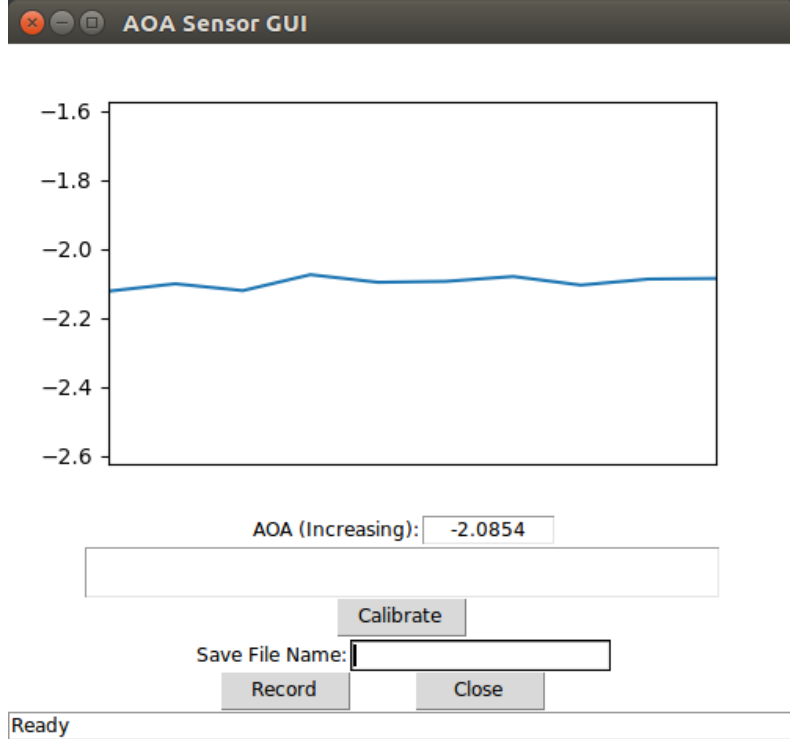


Figure 3.16: GUI created to view and record angle of attack.

the microphone signal. Orange-colored cotton tufts were used with a blue masking tape background as shown in Fig. 3.17. This particular color combination was used so that we could use computer vision to detect the length of the tuft at different angles of attack and to determine how much the tuft is fluttering at each angle of attack. After some iterations, we decided that this color combination will give the best contrast for the computer vision to see the tufts. To perform the computer vision analysis, ten images were captured at each angle of attack using an Olympus EM-10 digital camera. The images are captured at a high enough shutter speed to minimize the motion blur of the tufts in each image.

3.4 Vortex Generator Activation System

Vane-type vortex generators are used due to their simplicity and acceptance in the aviation industry. The VGs are in a counter-rotating common flow down vortex pair configuration (Fig. 1.3a) due to that configuration's effectiveness. A dimensioned image of one of the vortex generators is shown in Fig. 3.18.

The vortex generator activation system design started with a trade study on how we

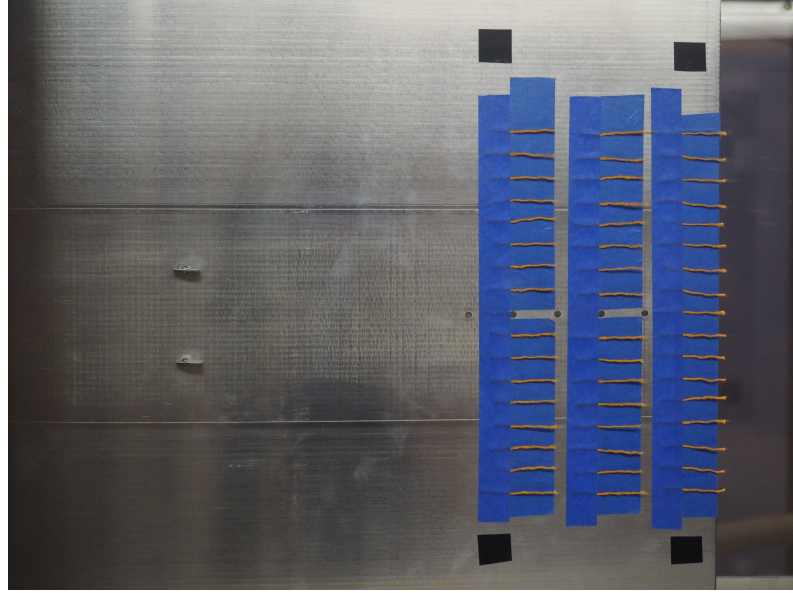


Figure 3.17: Tufts mounted near the wing's trailing edge.

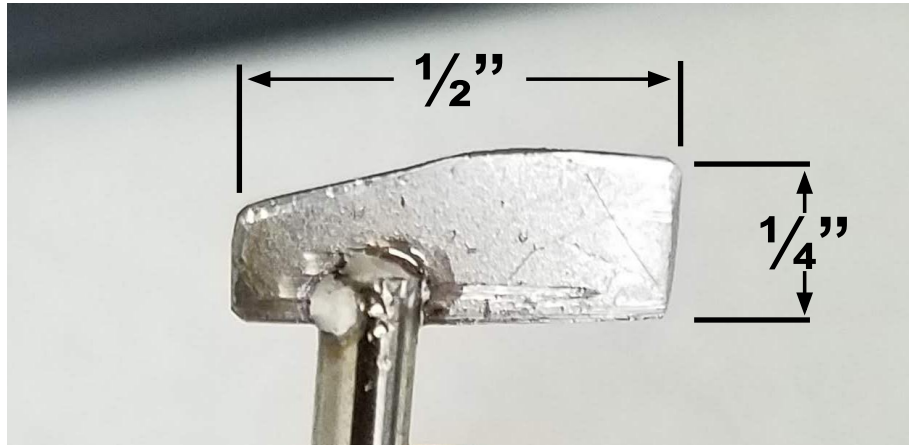


Figure 3.18: A vortex generator with major dimensions.

should activate the vortex generators (VG). Our two main choices were a pop-up design or a rotating design. For the pop-up design, the VGs would be stowed away so that they are flush with the wing surface. When boundary layer separation is detected, they would pop-up and start producing vortices. With the rotating design, the VGs start streamlined with the flow as to not produce vortices. This does incur an extra skin friction drag, but due to the size of the vortex generators this extra drag would be very small. To activate they would rotate to an angle of attack relative to the flow as shown in Fig. 3.19. While the pop-up design would mean slightly less drag in the stowed position, the rotating design

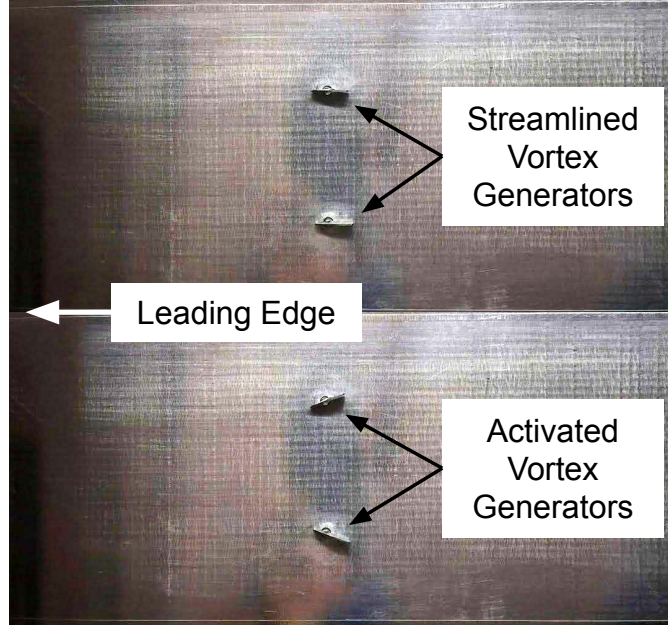


Figure 3.19: The vortex generators in their two different states.

was deemed to be easier to implement in the space available. This system used a small servo motor to rotate the vane-type VG to its active state. Since the holding torque of small servo motors is not very large, the VGs are rotated about their quarter-chord to minimize the torque exerted on the servo motor. The servo motors are mounted to a 3D printed tray that fits securely inside the center cutout in the wing section. Figure 3.20 shows an early prototype of the VG activation system mounted inside a wing section mock-up. A coupler was manufactured to attach the vortex generator to the servo motor. An Arduino Uno is used to control the servo motors and rotate the VGs to a fixed angle of 20° relative to the freestream velocity when the activation criterion is met. This angle was chosen based on convention.

3.5 Experiment Design

Once the wing model was finished and the microphone instrumentation was installed, the wind tunnel testing began. To ensure an efficient wind tunnel entry, we developed an experiment plan to follow during the testing phase. We developed this experiment plan to increase our understanding of the equipment and the physics of the flow at every step. The experiment plan has three main progression steps. The first step was to test the model

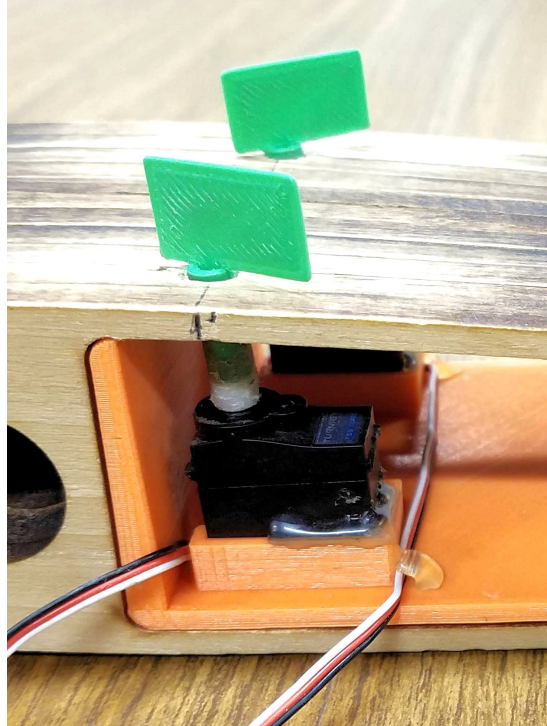


Figure 3.20: Early prototype of the servo motor tray and activation system.

and instrumentation and to determine how to best run the wind tunnel during subsequent tests. The next step was to build our understanding of the physics of the separating flow and determine an activation criterion. The final step was to test the activation criterion and activate vortex generators in a real-time experiment. An outline of the tests is shown in Table 3.1, and a detailed experiment list can be found in Appendix A.

Table 3.1: Outline of the wind tunnel tests performed and the purpose of each test.

Test #	Purpose
1	To test data acquisition systems, blow air over the model to check how the model behaves in the operational Alpha range, and test the Alpha readout
2	To achieve a lift curve for the NACA 0012 wind tunnel model without trip tape
3	To achieve a lift curve for the NACA 0012 wind tunnel model with trip tape
4	To take burst-mode microphone samples for averaging the FFT
5	To test whether the low frequency sounds at stall are from the air flow or from the model vibrations
6	To obtain a finer resolution alpha sweep around stall and to obtain photographs of the tufts during stall
7	To repeat Test #6 and to test for the zero lift angle
8	To test the tone generator setup through stall
9	To repeat Test #8 and test the tone generator setup through stall
10	To take pictures during stall for tuft analysis
11	To test the initial activation criterion
12	To test updated VG activation criterion, obtain measurements with activation system off and on, and to take tufts pictures

Chapter 4

Results and Discussion

4.1 Fluctuating Pressure Data

We began by inspecting the raw data that we recorded from each microphone during the alpha sweep. The data were analyzed using Python built-in packages. When the data were recorded, the sampling rate was not constant for every sample due to hardware inconsistencies. This would dramatically affect the Fast Fourier Transform (FFT) because the calculation assumes a constant sampling rate. To account for this, the data are resampled at a constant sampling rate of 8000 Hz. The data were recorded through the 12-bit analog-to-digital converter so the data need to be converted to volts. The FFT was then calculated using the SciPy FFT package. The power spectral density (PSD) is computed from the PSD output using Eq. 4.1 where FFT_{out} is the real values output from the FFT, F_s is the sampling frequency, and N is the number of samples.

$$PSD = |FFT_{out}|^2 \frac{1}{F_s N} \quad (4.1)$$

This results in a PSD with units of V^2/Hz . The PSD appeared to be very jagged, and it was difficult to determine what the peak frequency really was or the amplitude of that frequency. Figure 4.1 shows examples of the jagged PSDs obtained from the first low-speed test. The pressure fluctuations in the turbulent boundary layer are inherently unsteady, especially during separation, which means that the PSD varies from data set to data set. The jaggedness and unsteadiness of the PSD make it very difficult to study effectively without more data. To help account for this unsteadiness, we decided to time-average

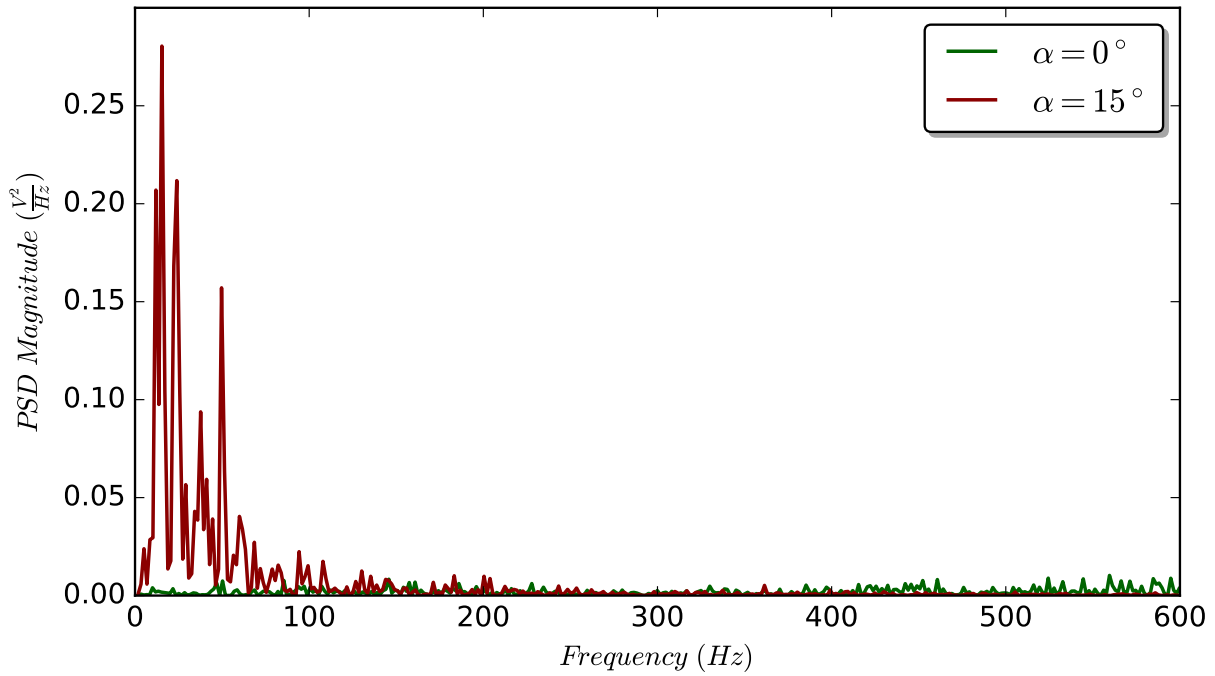


Figure 4.1: Comparison of the PSDs from MIC 4 at 0° angle of attack and 15° angle of attack obtained during the initial tests done at a Reynolds number of 400,000.

the PSD by taking multiple data sets of microphone data at each angle of attack. Fifteen data sets of 5000 samples were taken at each angle of attack. The same preprocessing is then performed on each data set, and a PSD is calculated for each data set. The 15 PSDs were then averaged together. This damps out the unsteadiness in the frequency domain and emphasizes the main frequencies present. To further damp out the unsteadiness in the frequency domain, a Savitzky-Golay Filter is applied to the PSD to smooth out the peaks of the PSD. After inspection of the averaged PSDs, a large increase in the power at frequencies below 400 Hz occurring during separation becomes apparent as seen in Fig. 4.2. Even the 1° change in angle of attack near stall produces a drastic change in the power level in the low frequency range. We expected this type of behavior based on Edelman's previous work [9], and also from our knowledge of the physics of a separating boundary layer. As the boundary layer gets close to separating, the dominant structures present in the flow will increase in size, resulting in lower frequency pressure fluctuations. This is the main characteristic of a separating boundary layer that we wanted to use as an activation criterion.

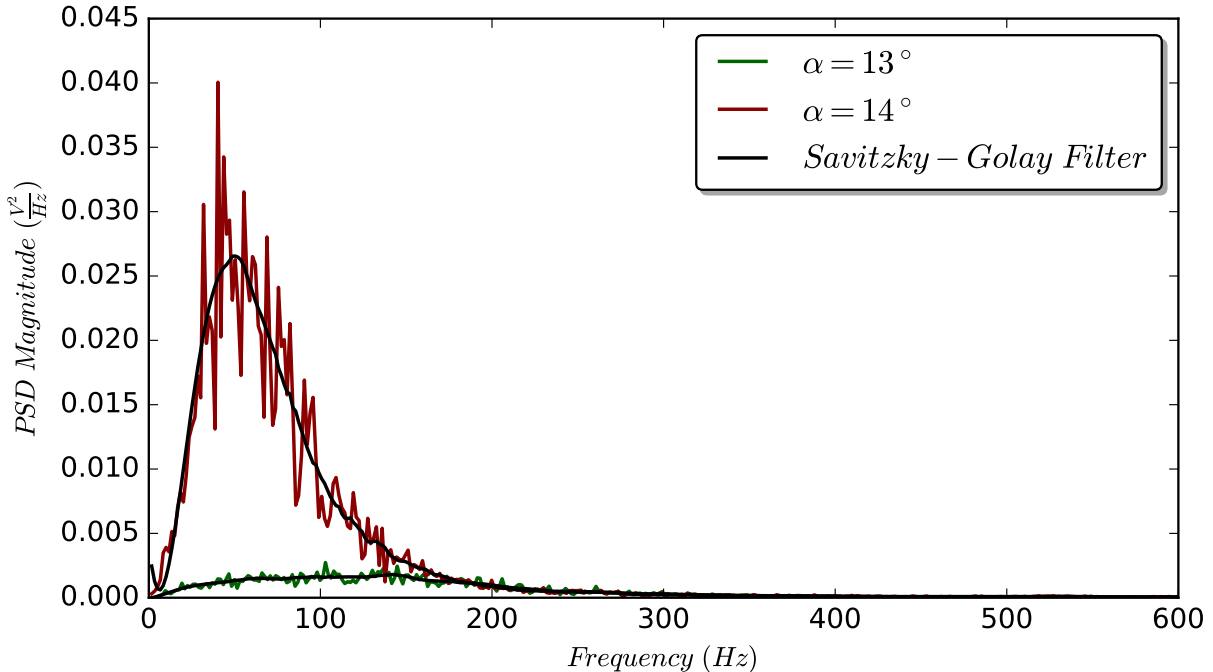


Figure 4.2: Comparison of the averaged PSDs from MIC 1 at 13° angle of attack and 14° angle of attack at a Reynolds number of 1,000,000.

While testing, we noticed that the model shakes violently at 15° angle of attack due to full stall on the wing. In order to confirm that the fluctuations recorded by the microphones are from the air and not the model, we performed tests with and without aluminum tape over the microphones. The aluminum tape is used to damp out the pressure fluctuations so that the primary source of fluctuations in the signal would be from the vibrations in the model. While the aluminum tape is not perfectly rigid and can let pressure fluctuations get to the microphone, it should damp out enough of the pressure fluctuations to show whether the primary low frequency fluctuations in the signal are from the model or the flow. As seen in Fig. 4.3, the large difference in the power levels showed us that the pressure fluctuations in the flow dominate the signal. This established confidence that we are recording the physical characteristics of the boundary layer and not mechanical vibrations. In order to confirm that the pressure fluctuations that we are recording are a result of the boundary layer separation, we use flow visualization to tell us when and where the boundary layer begins to separate.

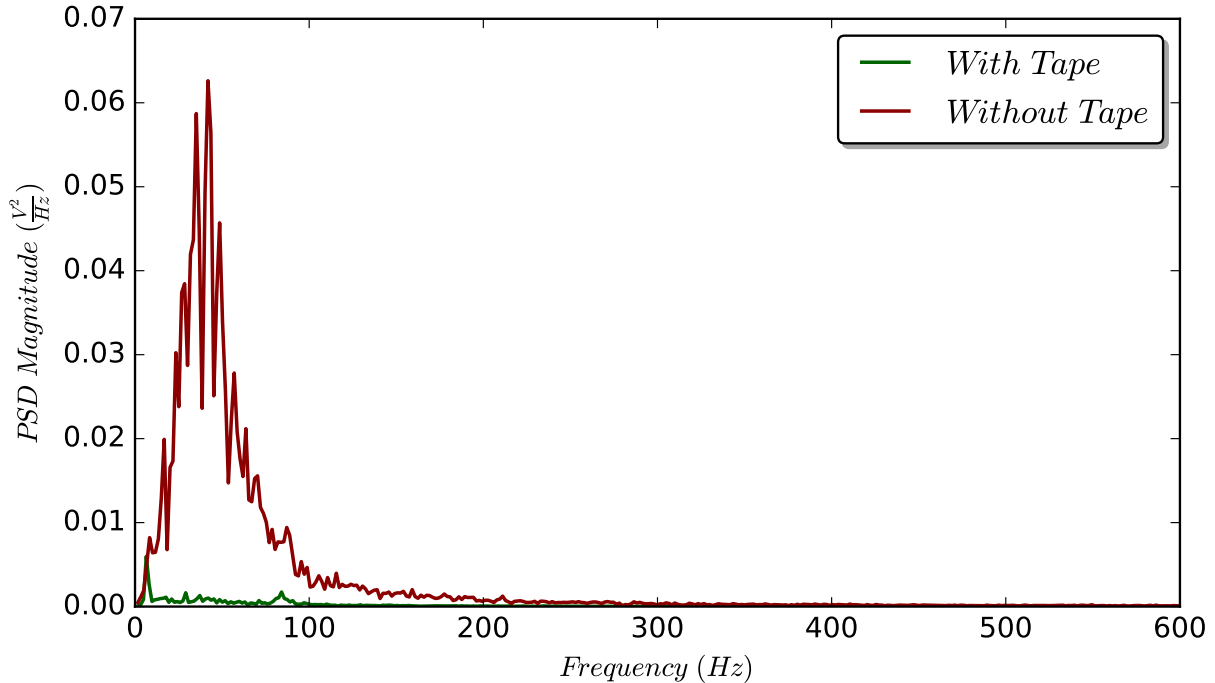


Figure 4.3: Comparison of the averaged PSDs from MIC 1 at 15° angle of attack with and without aluminum tape over the microphone at a Reynolds number of 1,000,000.

4.2 Separation Location Using Flow Visualization

While it can be difficult to determine a single separation point due to the unsteadiness of separation, it was important for us to have an idea where the separation point was located so that we could use that information to determine an activation criterion. As defined by Simpson, the boundary layer has four stages of detachment [31]. With tufts we are only able to determine the full detachment point with confidence. This will be where the tufts reverse and remain fully reversed the majority of the time. To accomplish this analysis, we took pictures of tufts mounted near the trailing edge during the tests, and undergraduate researchers Kilian Ginnell and Shannon Geary used computer vision to track the tufts in the pictures. Figure 4.4 shows their results from the computer vision analysis. The y-axis shows the length of the tufts in the streamwise direction. The smaller values mean that the tufts are experiencing reverse flow. This analysis is important as it tells us when the boundary layer is separating so that we can compare that information to the microphone data. This allows us to correlate changes in the microphone signals to the flow behavior. It should be noted how the boundary layer separation creeps upstream

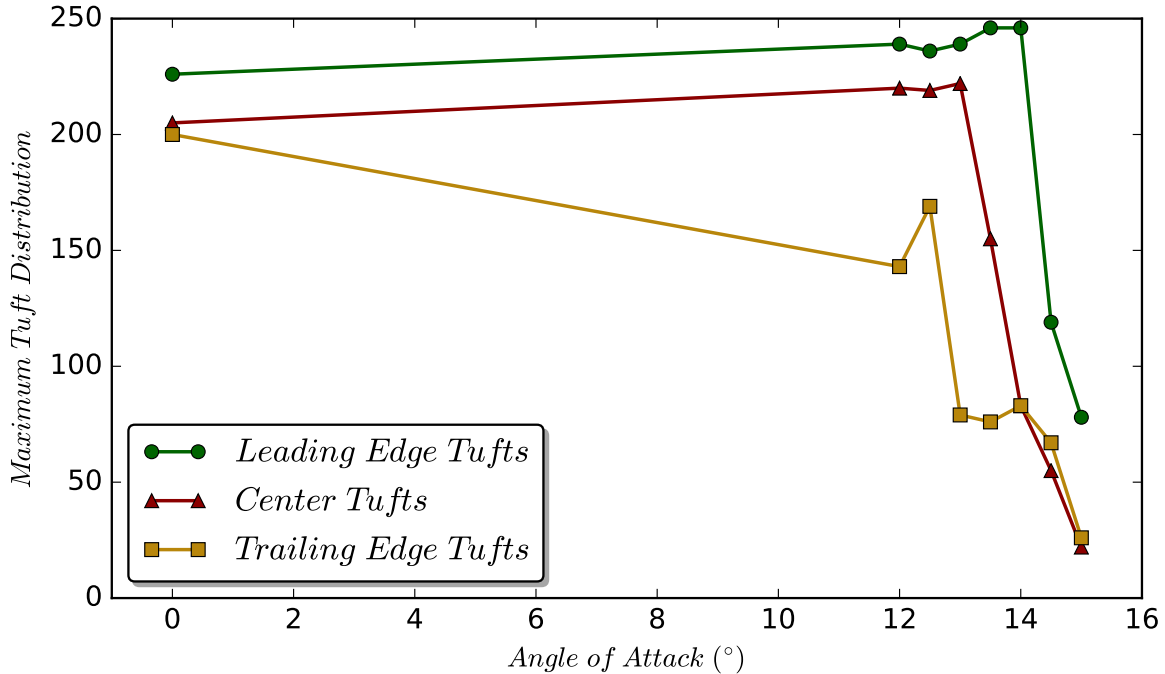


Figure 4.4: Results from the computer vision analysis of the tufts.

from the trailing edge. The trailing edge tufts start reversing earlier than the tufts closer to the leading edge. This is the expected behavior when the stall is of trailing-edge type [12], and we expect to see a similar behavior when analyzing the pressure fluctuation frequencies and magnitudes.

4.3 Power Spectrum Analysis

Once the averaged PSD was obtained, we plotted the peak frequencies and peak magnitudes at each angle for each microphone to see if there is a clear indicator of separation. The integral of the PSD over the frequency band 40 Hz - 400 Hz is also plotted. This integrated value corresponds to the signal power over that frequency range and has units V^2 . Figure 4.5 shows the results of the frequency domain analysis for all microphones where MIC 1 is the microphone closest to the trailing edge and MIC 5 is the microphone furthest from the trailing edge. It can be seen that the peak frequency values decrease to frequencies below 100 Hz at high angles of attack. All microphones converge to a single peak frequency when full stall occurs over the entire wing. This makes physical sense because all of the microphones are in the fully detached region and experiencing the same

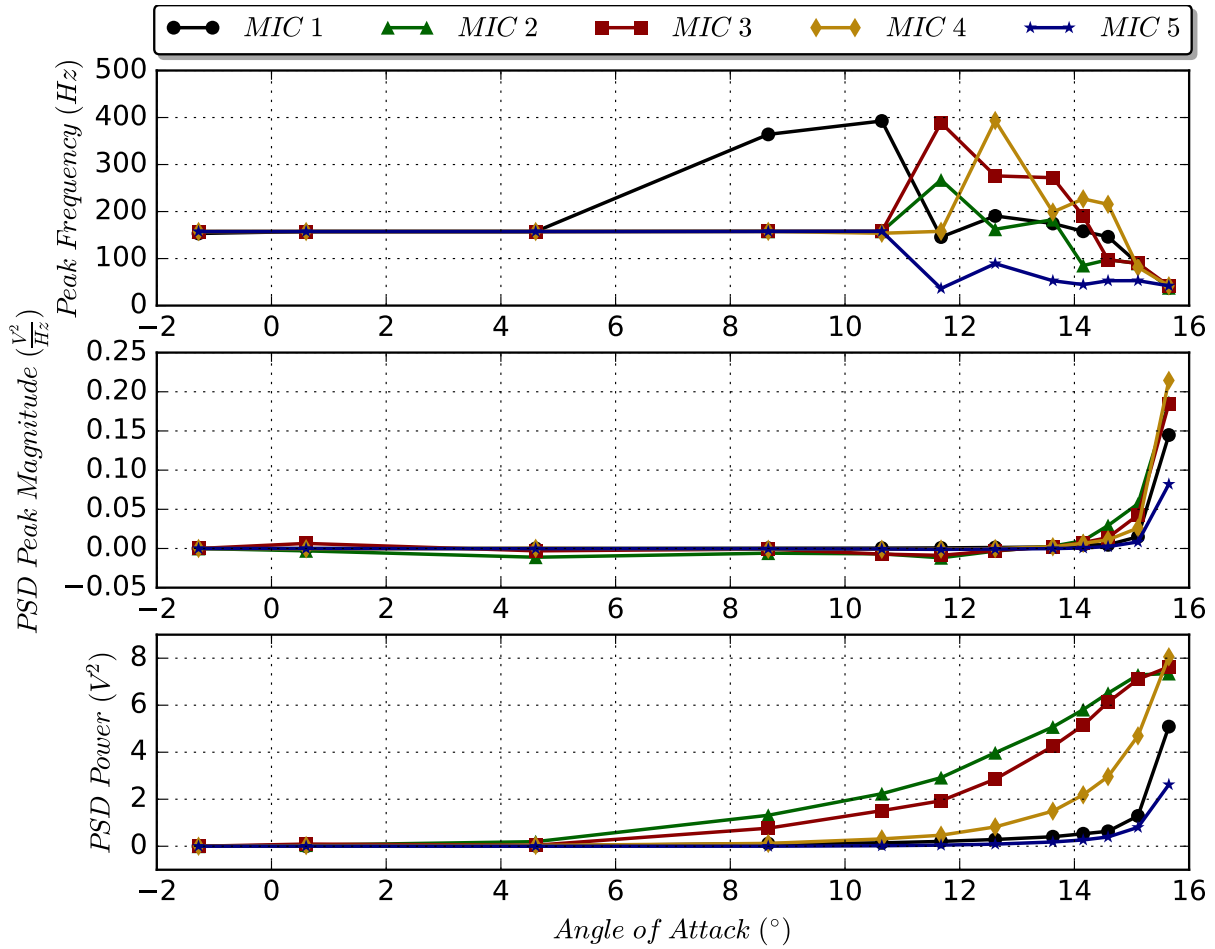


Figure 4.5: Peak frequency, PSD peak magnitude and PSD power plotted against the angle of attack for a Reynolds number of 1,000,000.

large separation structures.

Some strange behaviors are seen in the lower angles of attack where the frequencies jump between values around 160 Hz and 400 Hz. Figure 4.6 shows the FFT of the signal from MIC 1 at 0° angle of attack. There is a definite peak around 160 Hz, but the FFT is relatively flat and has smaller peaks at higher frequencies. Since the pressure fluctuations in a turbulent boundary layer are unsteady, the dominant frequency measured can vary with time. The order in which each microphone's frequency decreases does not show the expected trend. This could be because the Mach number is low and sound can travel upstream from the trailing edge. This means that all of the microphones can detect separation occurring downstream of their position. This explains why the tufts show the

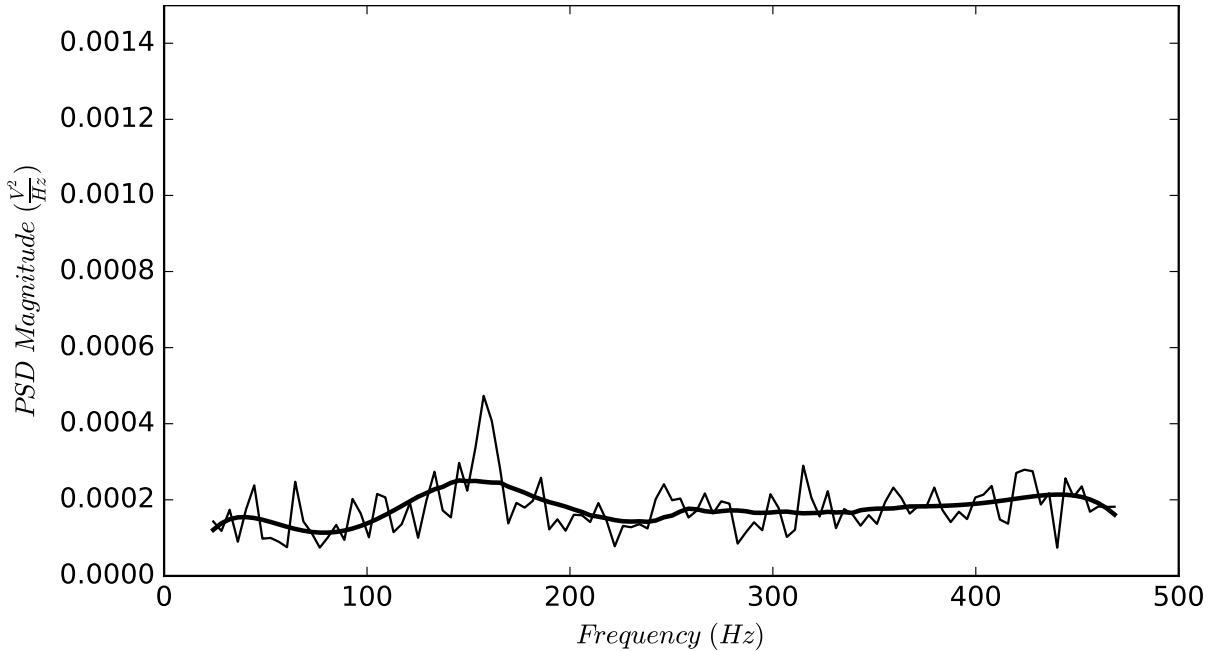


Figure 4.6: FFT of the MIC 1 signal at a Reynolds number of 1,000,000 and angle of attack of 0° .

separation marching upstream from the trailing edge, but the peak frequencies do not show the same behavior.

The peak magnitudes did not show the expected trend with respect to the microphone positions either. We expected that the peak magnitude of MIC 1 would be higher at a lower angle of attack than MIC 2 and so on. Instead, the point at which the peak magnitude begins to increase does not depend on the microphone's proximity to the trailing edge. This can be explained the same way as the peak frequency behavior. An additional explanation for why this occurred is the fact that we used automatic-gain amplifiers instead of fixed-gain amplifiers. This means that each microphone likely has a different gain so they cannot be directly compared. While this does not diminish the overall significance of the experiment, it does mean that we will not be able to use the comparison of signal magnitude between two or more microphones as a method of separation detection without further work. It is possible that we could try to normalize all the signals to the same scale, but without knowing the gain, it is hard to decide on the best way to do this. The best method of improving this will be to use fixed-gain amplifiers in the future and set all the gains to the same value. At this point, we shifted all of the

points so that the first point is equal to zero. This brings all of the microphones to the same scale so that we may compare them. It should be noted that all the microphones do have slightly different behaviors even when brought to the same scale. The behavior of each microphone does remain consistent with itself however.

An increase is seen at high angles of attack in both the peak magnitude values and the power values. In the case of the PSD power, the values increase more gradually as the wing approaches stall. Out of the five microphones, MIC 4 shows the most favorable behavior. The power levels of MIC 4 begin to increase more sharply between 12° and 14° which is where the tufts indicate separation beginning to occur locally to MIC 4. For this reason, MIC 4 was chosen as the microphone to be used to activate the vortex generators.

4.4 Determine Activation Criterion

Although a difference between the fully attached flow and fully separated flow can be seen in Fig. 4.5, there was not a clear indication of a separation point. We also noticed that the peak frequency value can behave sporadically, so the frequency alone should not be used as the primary determining factor for activation. While the peak magnitude is more stable, we still want some aspect of the frequency involved in the activation decision. This decreases the likelihood that an extraneous tone outside of the low frequency range could activate the vortex generators. As a compromise, we decided to use the area under the PSD curve over the important frequency band: 40 Hz - 400 Hz. This gives us the stability of the magnitude signal, but also a dependence on the frequency as we are only taking the integral over the frequency range that we are seeing a difference in as we approach separation. Plotted against the angle of attack, these integrated values appear to behave similarly to the peak magnitude values but are more robust to the unsteady nature of separated flow. To decide how many snapshots are needed for the activation system, we investigated how much the integrated value depends on the number of PSDs averaged and found that the number of windows averaged does not have a large effect on the integrated values. This was not true for the peak frequency and peak magnitude as the unsteady nature of separation causes these values to vary.

As previously mentioned, MIC 4 is used to activate the vortex generators. After inspecting the PSD power curve seen in Fig. 4.5, we decided to use a threshold value to activate the vortex generators. When the power level measured by MIC 4 is greater than the threshold value, the vortex generators are told to activate. This threshold is chosen based on the angle of separation according to the tuft analysis. Figure 4.4 shows that we should activate the vortex generators between 13° and 14° so a corresponding power level is chosen as the threshold value. While this method of choosing the activation criterion is not ideal, it works for this proof-of-concept. Ideally, the activation criterion would be completely independent of angle of attack. While the method used for this thesis involves angle of attack, the activation criterion still relies on the physical behavior of the boundary layer.

4.5 Real-Time VG Activation

The last part of the experiment was to demonstrate the ability to activate vortex generators in real-time and to show their effectiveness. The activation system needs to have a fast time response in order to be effective. That we were able to find an activation criterion that only needs a single PSD at a time means that the system can be kept very simple and fast. We can achieve response times close to a second rather than over 10 seconds which makes this system much more feasible for real-world applications.

Initial tests were run to verify that the system activated. For these initial tests, the vortex generators were only on while the PSD power was greater than the chosen threshold value. This led to an interesting behavior because when the vortex generators activated, the PSD power dropped below the threshold value causing the vortex generators to turn to their inactive position. This then caused the PSD power to increase again, and the vortex generators activated which resulted in the cycle repeating itself. On top of being an interesting behavior, this also provided confidence that the pressure fluctuations being measured were in fact due to boundary layer separation. While a deactivation method must be explored, this was not the focus of this thesis so the system was set to stay active once it was initially activated.



Figure 4.7: Tufts without the vortex generators turned to their active position.

Once it was demonstrated that the system worked, tests were performed to measure parameters that show the effectiveness of the active vortex generators. The PSD power and the lift coefficient with the active vortex generator system were plotted against angle of attack and compared to the results without the active vortex generator system.

The first indication of the system's effectiveness was the tuft's reaction to the active vortex generators. Figure 4.7 shows the tufts experiencing reverse flow when the vortex generators are not activated. Figure 4.8 shows how the tufts directly downstream of the vortex generator pair are not reversed like the surrounding tufts when the vortex generators are activated. This also shows how localized the effect of the vortex generators is. Since the microphones are also in the affected region, they also hear the effect of the vortex generators. Figures 4.9 and 4.10 show the PSD power with and without the active vortex generators. For both Reynolds numbers, the activation of the vortex generators causes a decrease in the PSD power in the low frequencies. This means that the large structures in the separation region are no longer present in the flow over the microphones. As the angle continues to increase, the power increases again. This is expected because the vortex generators are only able to delay but not prevent boundary layer separation.

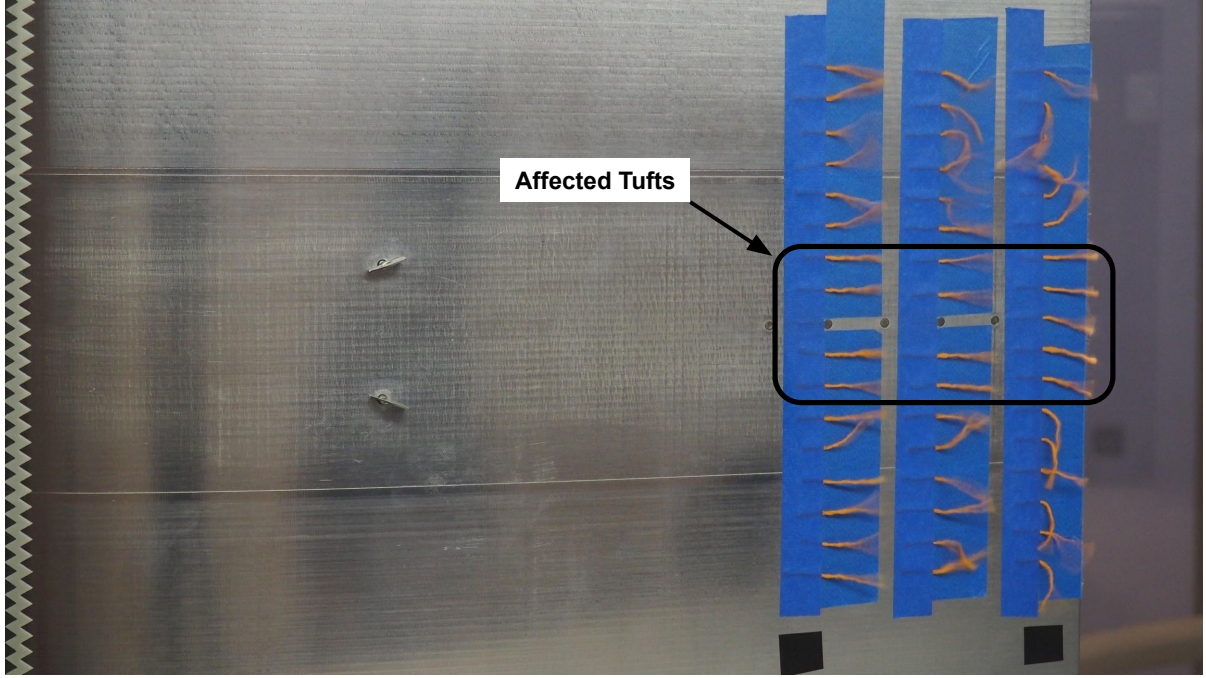


Figure 4.8: Tufts with the vortex generators turned to their active position.

The lift coefficient results are shown in the Figs. 4.11 and 4.12. These plots show the lift coefficient curves with and without the active vortex generators. We did not expect to see a noticeable effect on the lift coefficient as there was only a single vortex generator pair. A small increase in the maximum lift coefficient is seen in the case with the active vortex generators for both Reynolds numbers. Although only a small area is affected by the vortex generator pair, it is enough to provide an increase in $C_{L_{max}}$. With the active vortex generators, the $C_{L_{max}}$ improves 13.8% and 6.9% for Reynolds numbers of 500,000 and 1,000,000 respectively. These results show that the active vortex generator system does have a positive effect on the lift characteristics of the wing. Although more research is required, this proof-of-concept demonstrates that the active vortex generators are highly effective at delaying boundary layer separation.

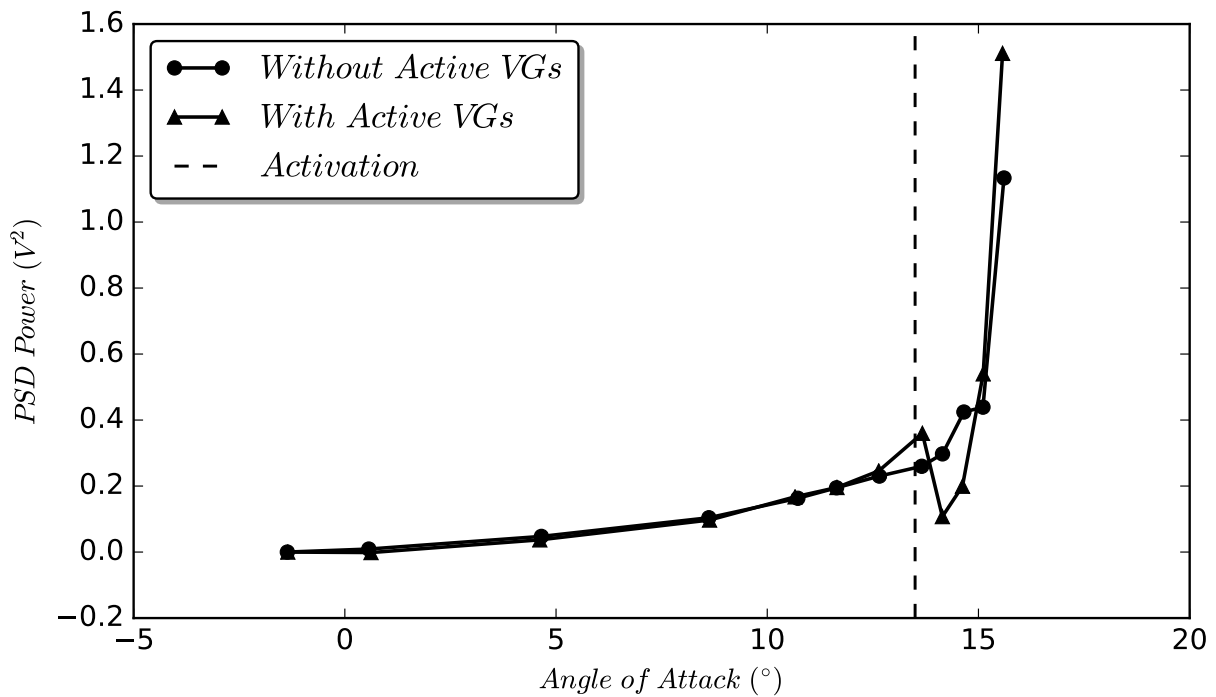


Figure 4.9: Comparison of the PSD power levels at a Reynolds number of 500,000 with and without active vortex generators (VGs).

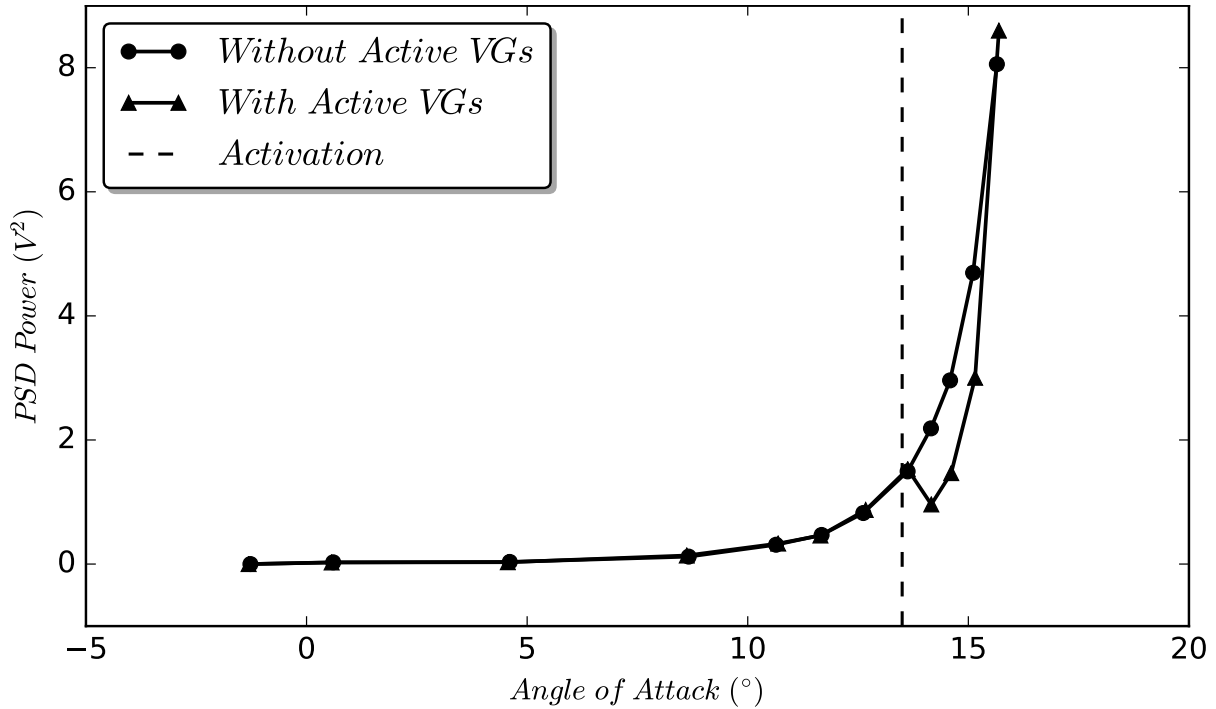


Figure 4.10: Comparison of the PSD power levels at a Reynolds number of 1,000,000 with and without active vortex generators (VGs).

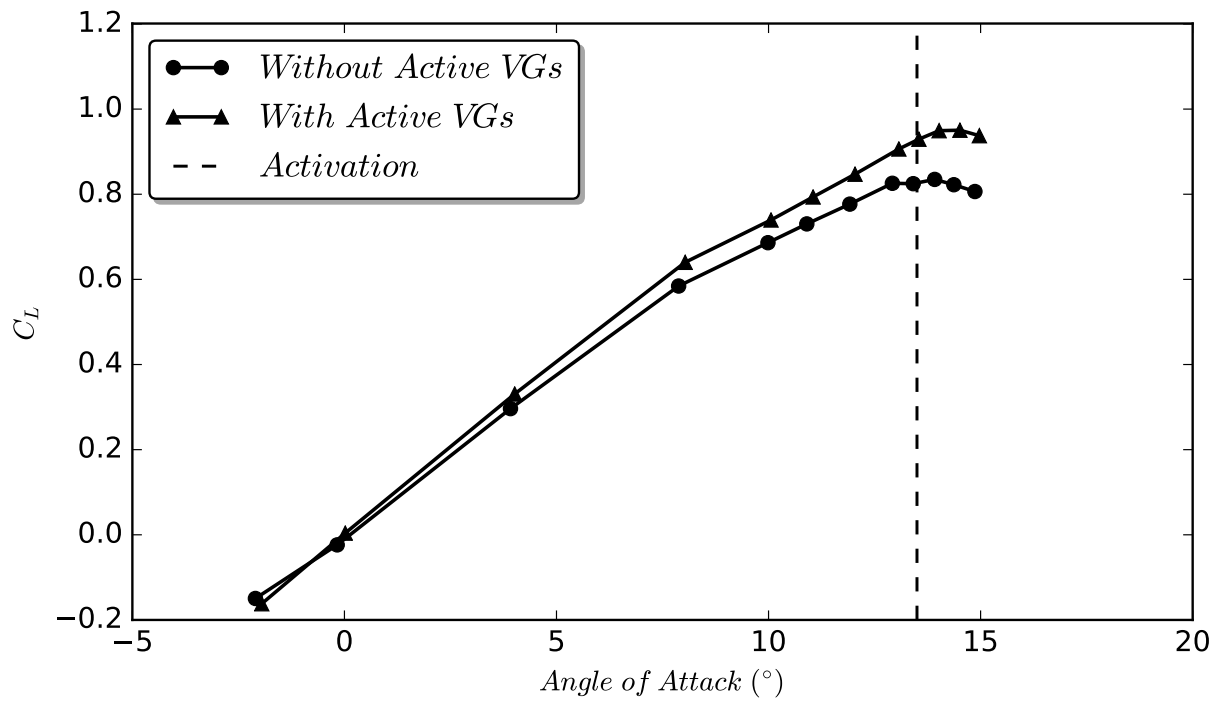


Figure 4.11: Comparison of the lift coefficient curves at a Reynolds number of 500,000 with and without active vortex generators (VGs).

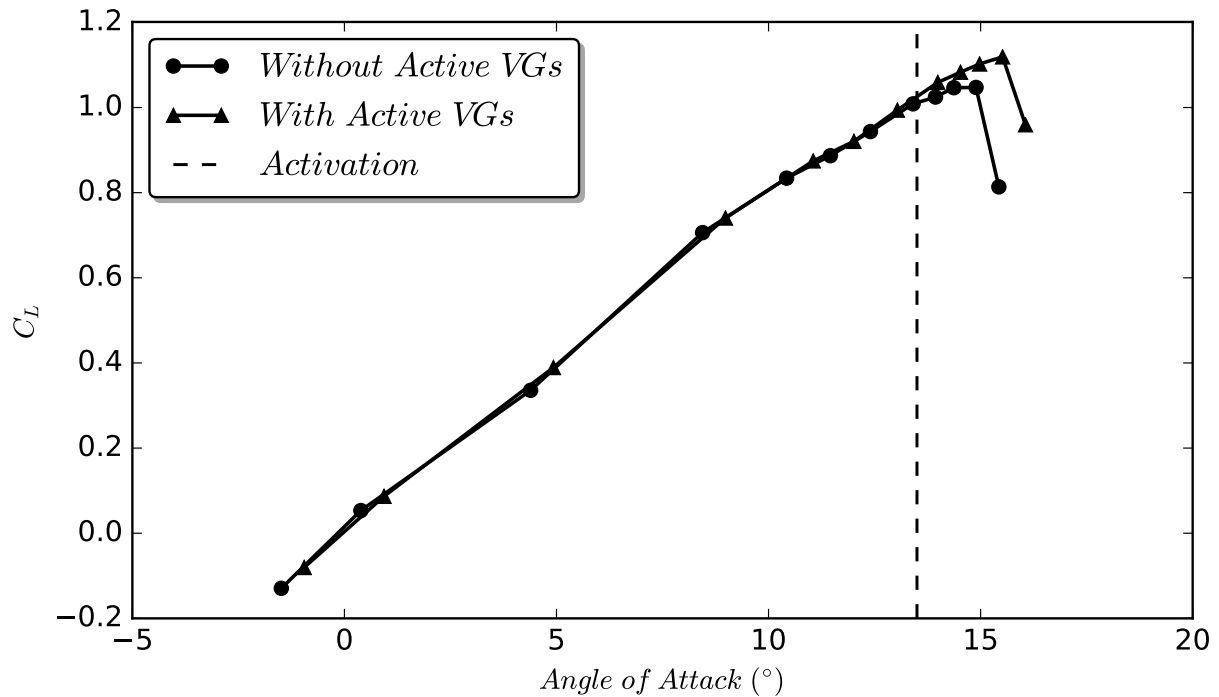


Figure 4.12: Comparison of the lift coefficient curves at a Reynolds number of 1,000,000 with and without active vortex generators (VGs).

Chapter 5

Conclusions and Future Study

5.1 Hypothesis Closure

This thesis aimed to answer the question: can inexpensive microphones be used to detect boundary layer separation and activate vortex generators to delay the boundary layer separation? Our research taught us that separating boundary layers have relatively large structures that lead to low frequency surface pressure fluctuations. These low frequency pressure fluctuations dominate the frequency spectra in a separated boundary layer, making them a possible early-warning indicator of boundary layer separation that microphones can sense. Current stall warning systems available on airplanes do not detect stall based on the physics of boundary layer separation, and a system that is able to reliably and quickly detect boundary layer separation would be valuable to the aerospace industry. Boundary layer separation can cause stall which accounts for nearly 25% of the fatal airplane accidents from 2000 through 2014 [15]. Stall is an issue that large airframe manufacturers are still trying to solve. Vortex generators are commonly used to delay boundary layer separation on aircraft, but they come with a parasitic drag penalty. An autonomous vortex generator system would increase aircraft safety without a drag penalty.

In order to answer the question proposed in this thesis, wind tunnel tests were conducted with a NACA 0012 wing section in a low speed wind tunnel. These tests were run at Reynolds numbers of 500,000 and 1,000,000. The microphone data collected were

analyzed for characteristics that could be used as activation criteria. Knowing that low frequency pressure fluctuations are present in a separating boundary layer, we decided to focus on the frequency characteristics of the microphone signals. We designed a data collection system to record the pressure fluctuations with the microphones. The analysis of the frequency spectra obtained showed that a difference between a fully attached boundary layer and a fully separated boundary layer is apparent, but there is not a clear indication of a separation point seen in the data. Since there is not an obvious indication of separation, an activation criterion is chosen by using the known angle of attack at which separation occurs. A threshold value of the power spectral density (PSD) energy level is found at the separation angle of attack and is used to activate the vortex generators. Although this path of research is still in its early stages, the results shown in this thesis indicate that an autonomous vortex generator system can activate and delay boundary layer separation in real-time.

5.2 Future Study

At this point in time, this boundary layer separation detection and VG activation system is a good proof-of-concept, but there is still a lot of work that can be done. More experiments must be done at different Reynolds numbers to further study the Reynolds number dependence in the pressure fluctuations. The Reynolds numbers of 500,000 and 1,000,000 tested in this thesis do not fully cover the range of flight Reynolds numbers.

It would also be valuable to investigate different activation algorithms. The current criterion has been demonstrated to work, but there are other options that could be more reliable. For example, Patel's research showed that the increase of standard deviation of the voltage signal from a microphone can also be used as an activation criterion [24]. This could be a valuable research path to take as the standard deviation could be scaled to be independant of Reynolds number.

Work should also be done to improve the design of the VG activation system. Currently, the system activates, but it is not fault-tolerant. For this system to be used in a real-world application, it would need to be much more tolerant to failures. This could start

with designing a system that would always fail with the VGs in an activated position, so boundary layer separation is still delayed at the cost of some additional drag. A valuable improvement would be to implement a reliable method of deactivating the VGs after stall has been prevented. Ideally, this would be independant of the pilot and based on the physics of the boundary layer, but this deactivation criterion would need to be just as reliable as the activation criterion. Prematurely deactivating the vortex generators could increase the chances that the pilot will be unable to recover from the stall. It could be that the best way to deactivate the system would be for the pilot to manually deactivate the VGs when the aircraft is back in a safe flight regime. This could be feasible as this task would not be time sensitive and would not add unsafe pilot workload.

Computational fluid dynamic models of the pressure fluctuations in the separation region should be constructed and compared to the experimental results. These models could then be used to predict the behavior of different airfoils. Having reliable CFD models would be useful for exploring many different test conditions quickly which can then guide future wind tunnel tests. Wind tunnel tests are time consuming and involved, and using CFD tests to guide wind tunnel tests can save time. There are many questions still to be answered concerning the detection of boundary layer separation, and both physical tests and simulation will be important for answering these questions.

This work and the tuft analysis work have been accepted into the 2020 AIAA Sci-Tech conference, and two papers will be presented at the conference in January 2020.

REFERENCES

- [1] W. R. Briley. A numerical study of laminar separation bubbles using the navier-stokes equations. *Journal of Fluid Mechanics*, 47(4):713–736, 1971.
- [2] T. F. Brooks and T. Hodgson. Trailing edge noise prediction from measured surface pressures. *Journal of sound and vibration*, 78(1):69–117, 1981.
- [3] M. Campbell, J. Cosgrove, C. Greated, S. Jack, and D. Rockliff. Review of lda and piv applied to the measurement of sound and acoustic streaming. *Optics & laser technology*, 32(7-8):629–639, 2000.
- [4] J. E. Carter. Inverse solutions for laminar boundary-layer flows with separation and reattachment. 1975.
- [5] D. Catherall and K. Mangler. The integration of the two-dimensional laminar boundary-layer equations past the point of vanishing skin friction. *Journal of Fluid Mechanics*, 26(1):163–182, 1966.
- [6] G. Comte-Bellot. Hot-wire anemometry. *Annual review of fluid mechanics*, 8(1):209–231, 1976.
- [7] DB Unlimited. *Electret Condenser Microphone*, 10 2013. Rev. 1.
- [8] L. East and W. Sawyer. An investigation of the structure of turbulent boundary layers. *Turb. Bound. Layers: Experiment, Theory and Modeling*, 1979.
- [9] L. M. Edelman, A. Pensado, S. K. Robinson, and C. P. Van Dam. Low-cost detection of boundary layer separation with dynamic pressure measurements. In *8th AIAA Flow Control Conference*, page 3623, 2016.
- [10] W. Froude. Experiments on the surface-friction experienced by a plane moving through water. *British Association for the Advancement of Science*, pages 138–146, 1872.
- [11] M. Gad-el Hak, A. Pollard, and J.-P. Bonnet. *Flow control: fundamentals and practices*, volume 53. Springer Science & Business Media, 1998.
- [12] D. E. Gault. A correlation of low-speed, airfoil-section stalling characteristics with reynolds number and airfoil geometry. 1957.
- [13] A. R. Group. Aeronautical wind tunnel specifications and schematics. <https://flight.engr.ucdavis.edu/facilities/aeronautical-wind-tunnel/>, Accessed 2019. [Online; accessed July-2019].
- [14] V. Gusmeroli and M. Martinelli. A novel concept in laser doppler velocimetry: the distributed ldv. In *5th International Meeting of IAHR (Intern. Ass. for Hydraulic Research)*, page 10, 1991.

- [15] D. J. Kenny. Stall and spin accidents: Keep the wings flying. https://www.aopa.org/-/media/media/aopa/home/pilot-resources/safety-and-proficiency/accident-analysis/special-reports/stall_spin.pdf, 2017. [Online; accessed July-2019].
- [16] S. J. Kline, W. C. Reynolds, F. Schraub, and P. Runstadler. The structure of turbulent boundary layers. *Journal of Fluid Mechanics*, 30(4):741–773, 1967.
- [17] J. Klineberg and J. Steger. On laminar boundary-layer separation. In *12th Aerospace Sciences Meeting*, page 94, 1974.
- [18] J. C. Lin, S. K. Robinson, R. J. McGhee, and W. O. Valarezo. Separation control on high-lift airfoils via micro-vortex generators. *Journal of aircraft*, 31(6):1317–1323, 1994.
- [19] C. G. Lomas. *Fundamentals of hot wire anemometry*. Cambridge University Press, 1986.
- [20] D. G. Mabey. Comment on “a review of research on subsonic turbulent flow attachment”. *AIAA Journal*, 20(11):1632b–1632b, 1982.
- [21] W. Merzkirch. *Flow visualization*. Elsevier, 1974.
- [22] J. NICKERSON, JR. A study of vortex generators at low reynolds numbers. In *24th Aerospace Sciences Meeting*, page 155, 1986.
- [23] R. L. Panton and J. H. Linebarger. Wall pressure spectra calculations for equilibrium boundary layers. *Journal of Fluid Mechanics*, 65(2):261–287, 1974.
- [24] M. P. Patel, C. P. Tilmann, and T. T. Ng. Active transparent stall control system for air vehicles. *Journal of Aircraft*, 40(5):993–997, 2003.
- [25] W. R. Pauley and J. K. Eaton. Experimental study of the development of longitudinal vortex pairs embedded in a turbulent boundary layer. *AIAA Journal*, 26(7):816–823, 1988.
- [26] L. Prandtl. Der luftwiederstand von kugeln. *Nachrichten von der Gesellschaft der Wissenschaften zu Göttingen, Mathematisch-Physikalische Klasse*, 1914:177–190, 1914.
- [27] L. Prandtl. Motion of fluids with very little viscosity. *NACA Translation No.452*, 1928.
- [28] M. Raffel, C. E. Willert, F. Scarano, C. J. Kähler, S. T. Wereley, and J. Kompenhans. *Particle image velocimetry: a practical guide*. Springer, 2007.
- [29] S. K. Robinson. Coherent motions in the turbulent boundary layer. *Annual Review of Fluid Mechanics*, 23(1):601–639, 1991.

- [30] G. Sessler and J. West. Electret transducers: a review. *The Journal of the Acoustical Society of America*, 53(6):1589–1600, 1973.
- [31] R. L. Simpson. Turbulent boundary-layer separation. *Annual Review of Fluid Mechanics*, 21(1):205–232, 1989.
- [32] R. L. Simpson, M. Ghodbane, and B. McGrath. Surface pressure fluctuations in a separating turbulent boundary layer. *Journal of Fluid Mechanics*, 177:167–186, 1987.
- [33] I. Tani. History of boundary layer theory. *Annual review of fluid mechanics*, 9(1):87–111, 1977.
- [34] J. C. Williams III. Incompressible boundary-layer separation. *Annual Review of Fluid Mechanics*, 9(1):113–144, 1977.

LIST OF SYMBOLS

δ Boundary layer thickness

ρ Density

σ Pressure source term

τ_M Maximum shear stress

$C_{L_{max}}$ Maximum lift coefficient

F_s Sampling frequency

FFT_{out} The real-value output of the Fast Fourier Transform

H Shape factor

N Number of samples

p Pressure

U Mean velocity

u Fluctuating velocity

U_∞ Freestream velocity

Appendices

Appendix A

Experiment Plan

Test #1

- Purpose

To test data acquisition systems, blow air over the model to check how the model behaves in the operational Alpha range, and test the Alpha readout.

- Hardware Required

NACA 0012 Wind Tunnel Model

Lift Balance

Teensy LC (AOA)

Teensy 3.5 (Microphones)

Laptop and cables

- Procedure Outline

Low Speed: Max 40-50 mph

Course Alpha Sweep: -5° - 15° in 5° increments

Note: Slowly increase AOA around stall. Observe model behavior.

Take AOA, mic, and lift balance data at each measurement

Total: 5 measurements

15 second sample per measurement

- **Time Required**

Total: about 1hr

- **Post-Test Notes**

Problems with AOA sensor code so set AOA using tick marks on turntable

Stall occurred around $13^\circ - 14^\circ$ according to tufts

Recorded force balance data and microphone data successfully.

Test #2

- **Purpose**

To achieve a lift curve for the NACA 0012 wind tunnel model without trip tape.

- **Hardware Required**

NACA 0012 Wind Tunnel Model

Lift Balance

Teensy LC (AOA)

Teensy 3.5 (Microphones)

Laptop and cables

- **Procedure Outline**

Test without trip tape

Reynolds Numbers: 500,000 and 1,000,000

Alpha Sweep $-3^\circ - 11^\circ$ in 1° increments

Alpha Sweep 11° - 15° in 0.5° increments

Total: 23 measurements per Reynolds Number

15 second Force Balance sample per measurement

Record AOA and Microphones at each measurement

- **Time Required**

Setup: 30min

$Re = 500,000$, without trip tape: 30min

$Re = 1,000,000$, without trip tape: 30min

Clean-up: 15min

Total: 1hr 45min

- **Post-Test Notes**

Test was completed successfully

Test #3

- **Purpose**

To achieve a lift curve for the NACA 0012 wind tunnel model with trip tape.

- **Hardware Required**

NACA 0012 Wind Tunnel Model

Lift Balance

Teensy LC (AOA)

Teensy 3.5 (Microphones)

Laptop and cables

- Procedure Outline

Test with trip tape

Reynolds Numbers: 500,000 and 1,000,000

Alpha Sweep -3° - 11° in 1° increments

Alpha Sweep 11° - 15° in 0.5° increments

Total: 23 measurements per Reynolds Number

15 second Force Balance sample per measurement

Record AOA and Microphones at each measurement

- Time Required

Setup: 30min

$Re = 500,000$, with trip tape: 30min

$Re = 1,000,000$, with trip tape: 30min

Clean-up: 15min

Total: 1hr 45min

- Post-Test Notes

Test was completed successfully

Test #4

- Purpose

To take burst-mode microphone samples for averaging the FFT.

- Hardware Required

NACA 0012 Wind Tunnel Model

Lift Balance

Teensy LC (AOA)

Teensy 3.5 (Microphones)

Laptop and cables

- Procedure Outline

Test with trip tape

Reynolds Numbers: 500,000 and 1,000,000

Alpha Sweep -2° - 10° in 2° increments

Alpha Sweep 10° - 15° in 1° increments

Total: 13 measurements per Reynolds Number

15 second Force Balance sample per measurement

Record AOA and Microphones at each measurement

- Time Required

Setup: 30min

$Re = 500,000$, with trip tape: 25min

$Re = 1,000,000$, with trip tape: 25min

Clean-up: 15min

Total: 1hr 35min

- Post-Test Notes

During 500,000 Re run at AOA of 2° , a $\sim 200\text{Hz}$ tone was heard

Test was completed successfully

Test #5

- Purpose

To test whether the low frequency sounds at stall are from the air flow or from the model vibrations.

- **Hardware Required**

NACA 0012 Wind Tunnel Model

Lift Balance

Teensy LC (AOA)

Teensy 3.5 (Microphones)

Tape

Laptop and cables

- **Procedure Outline**

Test with and without aluminum tape over the microphones

Reynolds Number: 1,000,000

Slow Alpha Sweep to 12° without measurements

Alpha Sweep 12° - 15° in 1° increments

Total: 4 measurements per condition

Record AOA and Microphones at each measurement

- **Time Required**

Setup: 25min

$Re = 1,000,000$, with tape: 10min

$Re = 1,000,000$, without tape: 10min

Clean-up: 15min

Total: 1hr

- **Post-Test Notes**

Test was completed successfully

Test #6

- Purpose

To obtain a finer resolution alpha sweep around stall and to obtain photographs of the tufts during stall.

- Hardware Required

NACA 0012 Wind Tunnel Model

Lift Balance

Teensy LC (AOA)

Teensy 3.5 (Microphones)

Laptop and cables

Camera and tripod

- Procedure Outline

Reynolds Number: 1,000,000

Take picture at 0°

Slow Alpha Sweep to 6° without measurements

Alpha Sweep 6° - 10° in 1° increments

Alpha Sweep 10° - 13° in 0.5° increments

Alpha Sweep 13° - 14° in 0.25° increments

Alpha Sweep 14° - 15° in 0.5° increments

Total: 17 measurements

Take pictures 10° - 15°

Record AOA and Microphones at each measurement

- Time Required

Setup: 30min

$Re = 1,000,000$: 35min

Clean-up: 15min

Total: 1hr 20min

- Post-Test Notes

Test was completed successfully

Test #7

- Purpose

To repeat Test #6 and to test for the zero lift angle.

- Hardware Required

NACA 0012 Wind Tunnel Model

Lift Balance

Teensy LC (AOA)

Teensy 3.5 (Microphones)

Laptop and cables

Camera and tripod

- Procedure Outline

Reynolds Number: 1,000,000

Take picture at 0°

Alpha Sweep -2° - 0° in 0.5° increments

Alpha Sweep 6° - 10° in 1° increments

Alpha Sweep 10° - 13° in 0.5° increments

Alpha Sweep 13° - 14° in 0.25° increments

Alpha Sweep 14° - 15° in 0.5° increments

Total: 25 measurements

Take pictures 10° - 15°

Record AOA and Microphones at each measurement

- Time Required

Setup: 30min

$Re = 1,000,000$: 55min

Clean-up: 15min

Total: 1hr 40min

- Post-Test Notes

Test was completed successfully

Test #8

- Purpose

To test the tone generator setup through stall.

- Hardware Required

NACA 0012 Wind Tunnel Model

Lift Balance

Teensy LC (AOA)

Teensy 3.5 (Microphones)

Laptop and cables

- Procedure Outline

Reynolds Number: 1,000,000

Alpha Sweep 6° - 10° in 1° increments

Alpha Sweep 10° - 13° in 0.5° increments

Alpha Sweep 13° - 14° in 0.25° increments

Alpha Sweep 14° - 15° in 0.5° increments

Total: 17 measurements

Record AOA and Microphones at each measurement

- **Time Required**

Setup: 30min

$Re = 1,000,000$: 45min

Clean-up: 15min

Total: 1hr 30min

- **Post-Test Notes**

Tone generator was too quiet and was not heard by the microphones

Test #9

- **Purpose**

To repeat Test #8 and test the tone generator setup through stall.

- **Hardware Required**

NACA 0012 Wind Tunnel Model

Lift Balance

Teensy LC (AOA)

Teensy 3.5 (Microphones)

Laptop and cables

- **Procedure Outline**

Reynolds Number: 1,000,000

Alpha Sweep 6° - 10° in 1° increments

Alpha Sweep 10° - 13° in 0.5° increments

Alpha Sweep 13° - 14° in 0.25° increments

Alpha Sweep 14° - 15° in 0.5° increments

Total: 17 measurements

Record AOA and Microphones at each measurement

- **Time Required**

Setup: 30min

$Re = 1,000,000$: 45min

Clean-up: 15min

Total: 1hr 30min

- **Post-Test Notes**

Tone generator speaker blew out

Test #10

- **Purpose**

To take pictures during stall for tuft analysis.

- **Hardware Required**

NACA 0012 Wind Tunnel Model

Lift Balance

Teensy LC (AOA)

Teensy 3.5 (Microphones)

Tape

Laptop and cables

Camera and tripod

- Procedure Outline

Reynolds Number: 1,000,000

Measurement at 0°

Alpha Sweep 12° - 15° in 0.5° increments

Total: 8 measurements

Record AOA, Force Balance, and Pictures at each measurement

- Time Required

Setup: 15min

Re = 1,000,000: 30min

Clean-up: 15min

Total: 1hr

- Post-Test Notes

Test was completed successfully

Test #11

- Purpose

To test the initial activation criterion.

- Hardware Required

NACA 0012 Wind Tunnel Model

Lift Balance

Teensy LC (AOA)

Teensy 3.5 (Microphones)

Tape

Laptop and cables

Camera and tripod

- Procedure Outline

Reynolds Number: 1,000,000

Alpha Sweep -2° - 15°

Record video during sweep

- Time Required

Setup: 15min

$Re = 1,000,000$: 15min

Clean-up: 15min

Total: 0.75hr

- Post-Test Notes

First activation criterion unsuccessful. Corrected

Change code to activate vortex generators and keep activated

Test #12

- Purpose

To test updated VG activation criterion, obtain measurements with activation system off and on, and to take tufts pictures.

- Hardware Required

NACA 0012 Wind Tunnel Model

Lift Balance

Teensy LC (AOA)

Teensy 3.5 (Microphones)

Laptop and cables

Camera and tripod

- **Procedure Outline**

Reynolds Number: 1,000,000

Do a run with the activation system off and a run with the system on

Alpha Sweep 0° - 8° in 4° increments

Alpha Sweep 10° - 15° in 0.5° increments

Total: 11 measurements per condition

Record AOA, Microphones, and Pictures at each measurement

- **Time Required**

Setup: 30min

$Re = 1,000,000$: 45min

Clean-up: 15min

Total: 1hr 30min

- **Post-Test Notes**

Test was completed successfully